Disentangling the roles of subducted volatile contributions and mantle source heterogeneity in the production of magmas beneath the Washington Cascades

Walowski, K.J. [1*], Wallace, P.J. [2], DeBari, S.M. [1], Wada, I.,[3] Shaw, S.D. [4], Rea, J. [2]

[1] *Western Washington University, Bellingham WA USA*

[2] *University of Oregon, Eugene, OR USA*

[3] *University of Minnesota Twin Cities, Minneapolis, MN USA*

[4] *Weston and Sampson Engineers, Inc., Waterbury VT, USA*

**Corresponding Author*

Contact Information: walowski@wwu.edu

Keywords

basalt, mantle, subduction, volatiles

Key Points:

- The Washington Cascades sub-arc mantle is remarkably heterogeneous.
- Volatile contributions from the slab are identifiable across different magma types present in the WA Cascades.
- Fluid salinity variability and partial slab melting, non-uniquely, may contribute to subduction components along the entire arc.

Abstract

The compositional diversity of primitive arc basalts has long inspired questions regarding the drivers of magmatism in subduction zones, including the roles of decompression melting, mantle heterogeneity, and amount and compositions of slab-derived materials. This contribution presents the volatile (H_2O, Cl, and S), major, and trace element compositions of melt inclusions from basaltic magmas erupted at three volcanic centers in the Washington Cascades: Mount St. Helens (two basaltic tephras, 2.0–1.7 ka), Indian Heaven Volcanic Field (two <600 ka basaltic hyaloclastite tuffs), and Glacier Peak (late Pleistocene to Holocene basaltic tephra from Whitechuck and Indian Pass cones). Compositions corrected to be in equilibrium with mantle olivine display variability in Nb and trace element ratios indicative of mantle source variability that impressively span nearly the entire range of arc magmas globally. All volcanic centers have magmas with H_2O and Cl contributions from the downgoing plate that overlap with other Cascade Arc segments. Volatile abundances and trace element ratios support a model of melting of a highly variably mantle wedge driven by a subduction component of either variably saline fluids and/or partial slab melts. Magmas from Glacier Peak have Th/Yb ratios similar to Lassen region basalts, which may be consistent with contributions of "subcreted" metasediments not found in central Oregon and southern Washington magmas that overly the Siletzia Terrane. This dataset adds to the growing inventory of primitive magma volatile concentrations and provides insight into spatial distributions of mantle heterogeneity and the role of slab components in the petrogenesis of arc magmas.

1. Introduction

Fluid-flux melting of the mantle wedge is commonly attributed to be the primary driver of magmatism in arcs globally (Anderson, 1974; Fyfe and McBirney, 1975; McBirney, 1969; Sisson and Grove, 1993); however, decompression melting, mantle heterogeneity, and the amount and compositions of subducted materials (fluids vs. melts; crust vs. sediments), have all been suggested to play a role in producing the compositional diversity of primary basaltic magmas (e.g., Gill,1981; Elliott et al.,1997; Class et al., 2000). The Cascade volcanic arc (Fig. 1) has been described as a "hot" endmember arc worldwide in terms of subducting plate temperature (e.g., Green and Harry, 1999; Leeman et al., 2005a), and its unique thermal structure and along arc variability in downgoing and overriding plate parameters has prompted debate

about the relative roles of fluid/melt-flux melting versus decompression melting in petrogenesis (Ruscitto et al., 2012; Leeman et al., 2020). To better constrain the role of subduction-derived volatiles in arc magma petrogenesis, numerous studies have utilized the volatile composition of basaltic melt inclusions hosted in olivine. In the southern Cascades, melt inclusion work at Mount Shasta and Medicine Lake has revealed the low-H_2O (<1 wt.%), nearly anhydrous nature of LKT magmas, predominantly in the back-arc, and the wet (up to 5 wt.% H_2O) nature of calc-alkaline basalt and basaltic-andesite (CAB) magmas (Anderson, 1974; Le Voyer et al., 2010; Sisson and Layne, 1993). In the central arc (Oregon), the melt inclusion study of Ruscitto et al. (2010b) showed that CAB magmas have H_2O contents of 1.5-3.4 wt.% and trace element systematics suggestive of a smaller amount of slab-derived material added to the mantle wedge when compared to arc averages globally. Data from melt inclusions and bulk rock radiogenic isotopes for the Lassen Region of the southern Cascades support a model of mantle melting driven by a hydrous slab melt that involves fluids from the serpentinized upper mantle portion of the subducting plate and partially-melted oceanic crust (Walowski et al, 2015; Walowski et al., 2016). Melt inclusion studies in the northern Cascades have suggested that the enriched nature of magmas in the Garibaldi Volcano Group result from a slab tear at the northern termination of the subducting Juan de Fuca Plate, whereas more typical melting of depleted MORB mantle modified by fluids derived from the downgoing slab occurs beneath northern Washington (Shaw, 2011; Venugopal et al., 2020).

In this contribution, we present the volatile, major, and trace element compositions of melt inclusions hosted in high-Fo olivine from basaltic magmas erupted at three different volcanic centers in the Washington Cascades: Mount St. Helens, Indian Heaven Volcanic Field, and Glacier Peak (Fig. 1). We aim to disentangle the role of materials derived from the subducting slab from the role of mantle heterogeneity in the petrogenesis of arc magmas through this comparison of primitive basalts at the scale of both individual volcanic centers to ~300 km along this well-studied warm slab endmember active subduction zone.

2. Geologic Setting and Sample Localities

2.1 The Cascade Arc in Washington

The Cascades volcanic arc extends for ~1250 km from southern British Columbia to northern California along the west coast of North America (Fig. 1). Volcanism in the region results from the easterly subduction of the Juan de Fuca, Gorda, and Explorer oceanic plates beneath the North American continent. The Cascade Arc is subdivided into two main geographical segments, the High Cascades in the south and Garibaldi Volcanic Belt (GVB) in the north, by a change in the strike of the arc axis in the vicinity of Glacier Peak that follows a bend in the trench (Fig. 1). However, the Cascade Arc has been further segmented by various authors on the basis of volcano type, physical separations, and geochemistry (e.g., Guffanti and Weaver, 1988; Hildreth, 2007; Schmidt et al., 2008; Pitcher and Kent, 2019). Pitcher and Kent (2019) divide the arc into six regions which includes the Garibaldi (49.75–51 N), Baker (48.5–49.75 N), Glacier Peak (47.75–48.5 N), Washington (45.75–47.75 N), Graben (44.25–45.75 N), and South (41.25–44.25 N) Segments. Although this segmentation identifies volcanoes investigated in this study as from the Glacier Peak and Washington segments, in this contribution, we refer to the three volcanic centers as all within the WA Cascades on the basis of geographic location in the state of Washington, USA.

The Washington Cascades present a unique natural laboratory to explore spatial variability in the mantle sources and slab process that drive the geochemical diversity of primary arc magmas. The three major compositional types of primitive magmas identified in the Cascades are all found in this region: calc-alkaline basalts and basaltic-andesites (CAB), low potassium olivine tholeiites (LKT), and ocean island basalt (OIB)-like basalts [also referred to as intraplate basalt, IPB, or HFSE-rich)(Bacon, 1997; Borg et al., 1997; Conrey et al., 1997; Green and Harry, 1999; Leeman et al., 2005a; Reiners, 2000). In this study, we analyzed melt inclusions from three different volcanic centers with representatives of each of these three magma types.

Mount St. Helens (MSH) is located in southern Washington and represents the western edge of an east-to-west trending series of volcanic vents extending ~160 km (Hildreth, 2007). The longitudinal extent of Quaternary volcanism in this portion of the Cascades is anomalously broad, featuring both well-developed forearc (MSH, Indian Heaven Volcanic Field) and backarc (Simcoe Volcanic Field) volcanic centers. The breadth of the arc has been attributed to pull-apart geometries due to shear deformation resulting from the change in stress state from transtensional in the south to transpressive in the north (Humphreys and Grunder, 2022). The main arc axis at

this latitude (~46°N) is located at the approximate longitude of a second active stratovolcano, Mt. Adams, while MSH is situated 50 km to the west. The Indian Heaven Volcanic Field is situated in between these two prominent long-lived volcanoes (Fig. 1). The southern Washington Cascades is the only segment of the arc where two stratovolcanoes occur at the same latitude, and interestingly, MSH is the most western stratovolcano in the Cascades relative to the main arc axis. This region is part of the southern Washington and northern Oregon Cascade segments that are also unique for their geochemically distinct basement rock of oceanic plateau origin, the Siletz terrane (Church et al., 1986; Schmidt et al., 2008).

Glacier Peak is often considered the southernmost volcano in the northern segment of the Cascades, the Garibaldi Volcanic Belt (GVB). The GVB is ~330 km long, beginning just south of Glacier Peak and ending at Mt. Meager in British Columbia (Fig. 1). In this segment, quaternary volcanic output is low (see Hildreth, 2007), vents are sparse, and there is no eruptive activity noted in the forearc and backarc regions. While geographically part of the GVB, Mullen et al. (2017) suggest based on Pb isotope geochemistry that Glacier Peak should be reclassified as the northernmost large volcano of the High Cascades, whereas Pitcher and Kent (2019) suggest that Glacier Peak is a unique segment of the arc. The crust in the Glacier Peak and northern Washington Cascades region is composed predominantly of metamorphosed oceanic terranes (Brown, 1987) between 40-45 km thick (e.g., Ramachandron, 2006).

2.2 Sample Localities

2.2.1 Mount Saint Helens- Castle Creek Basalts

Mount St. Helens is one of the youngest and most active major volcanic centers in the Cascades—while volcanism at MSH extends back at least 300 ka, the majority of its volume has been erupted in just the past 28 kyr (Hildreth, 2007). Much of this recent eruptive activity, including the historical eruption of May 18, 1980, has been highly explosive, producing over 100 distinct tephra deposits (Mullineaux, 1996). This tephra is dominantly dacitic or rhyodacitic, and less commonly andesitic in composition.

Only one basaltic tephra sequence has been identified from the past 40 ka of explosive history at MSH: the ~1.7 ka Bu tephra erupted at the end of the Castle Creek eruptive period (2.0–1.7 ka). This unit consists of three chemically distinct, olivine-bearing lapilli and ash

deposits, referred to as Bu-1 (oldest), Bu-2 and Bu-3 (youngest) of OIB-type compositional affinity (Mullineaux, 1996; Clynne et al., 2008; Wanke et al., 2019). Also erupted during the Castle Creek period are basaltic lava flows of LKT affinity contemporaneous in age with Bu-1 tephra units (the Pre-Cave and Cave Basalts; Wanke et al., 2019), which indicates variability in parental basaltic magmas at MSH. From this eruption stratigraphy, only Bu-2 and Bu-3 provided tephra samples with olivine suitable for the melt inclusion work of this study. The whole rock major, trace element, and isotopic data compilation of Wanke et al. (2019) suggest the HFSE-rich, OIB-type Bu-2 and Bu-3 basalts we investigate here were generated in the periphery of the main mantle melting column, where lower degrees of partial melting produce magmas with higher concentrations of incompatible elements.

2.2.2 Indian Heaven Volcanic Field

Indian Heaven is a Quaternary mafic volcanic field located southeast of Mount St. Helens and southwest of Mount Adams (Fig. 1). The region is characterized by mafic shields and cones dominantly oriented along N-S trending zones of coalescing volcanic centers erupted between ~600 ka and ~8 ka (Korosec, 1989). The impact of alpine glaciation events during this time is notable, with evidence of subglacial emplacement (e.g., pillow lavas and hyaloclastites) and post-eruptive glacial erosion that has dissected numerous volcanic centers, resulting in large areas being covered by till and glacial outwash deposits (Smith, 1984; Korosec, 1989). Two samples collected from the region, the Basalt of Burnt Peak (QVBP) and the Basalt of Tillicum Creek (QVTC), contain high-Fo olivine with glassy melt inclusions suitable for analysis. Sample QVBP is a low-K olivine basalt collected from a thick (3-5 m) hyaloclastite tuff comprised of glassy scoria and coarse ash above a very thick pillow basalt unit. Sample QVTC, collected from a roadcut 3+ m section of palagonite tuff, is a medium-K olivine-rich basalt and has been identified as the most mafic in the volcanic field (Korosec, 1989).

2.2.3 Glacier Peak

Glacier Peak, the southernmost GVB volcanic center, is a dacitic stratovolcano that has been active for the past 700 ka (Tabor and Crowder, 1969). Low-K olivine tholeiite and calc-alkaline basalt tephras erupted near Glacier Peak at the Whitechuck and Indian Pass cinder cones, respectively, were sampled for this study. Whitechuck LKT tephras are generally aphyric,

with ≤5% phenocrysts dominated by olivine with minor plagioclase and groundmass clinopyroxene. Indian Pass CAB tephras have a slightly higher percentage of phenocrysts (≤10%), dominated by olivine phenocrysts (~7%), minor plagioclase, and a groundmass with plagioclase and clinopyroxene (Taylor, 2001).

The data presented in this contribution are a re-evaluation of the data presented in Shaw (2011). Based on whole-rock analyses and mineral chemistry, Taylor (2001) established that these two magmas are likely derived from two distinct mantle sources: the Whitechuck LKT from depleted mantle, similar to mid-ocean ridge basaltic sources (MORB), and the Indian Pass CAB from a more enriched source. All lavas have the characteristic high large ion lithophile elements (LILE) and high field strength (HFSE) indicative of variable amounts of addition of a hydrous subduction input (Taylor, 2001; Shaw, 2011). Radiogenic isotope compositions of the Indian Pass CAB overlap with the least radiogenic High Cascades samples and are suggested to record a relatively sediment-dominated subduction component, whereas the Whitechuck LKT has compositions more indicative of a subduction component dominated by oceanic crust fluids/melts, similar to that found in other GVB magmas (Mullen and Weiss, 2017).

3. Methods

3.1 Sample Preparation

Olivine crystals from the six tephra samples in this study were hand-picked, individually mounted in crystal bound on round glass slides, and doubly polished to expose melt inclusions on two parallel sides of the host olivine. Melt inclusions were glassy, between 50 and 150 microns in diameter, generally round or ellipsoidal, and contained vapor bubbles. After polishing, crystal bond was dissolved in acetone to remove the host olivine crystals from glass slides for Fourier Transform Infrared Spectroscopic (FTIR) analysis. After FTIR analysis, olivine hosts were washed and mounted in epoxy resin for electron probe micronalysis (EPMA) and Laser Ablation Inductively Coupled Mass Spectrometry (LA-ICP-MS).

3.2 Analytical Methods

3.2.1 FTIR

Analysis of H_2O and CO_2 in the melt inclusions was performed with a Thermo-Nicolet Nexus 670 FTIR spectrometer at the University of Oregon. Each unmounted olivine crystal was

individually placed upon a NaCl wafer. Spectral analyses were repeated between three and four times, each analysis encompassing 256 individual scans. Aperture size ranged from 50–120 μm depending on inclusion diameter. Inclusion thickness, initially determined with a digital micrometer measurement of the olivine wafer, was corroborated through the use of reflectance fringes. Thickness measurements typically agreed to within 5%, and calculated measurements were used in almost all cases. In cases in which the fringes were indistinct the initial micrometer measurement was used. The H_2O and CO_2 concentrations were calculated using the Beer-Lambert law (Dixon and Pan, 1995). Because the shape of the background in the region of the carbonate doublet is complex, it is necessary to subtract a carbonate-free reference spectrum to obtain a flat background. We measured absorbance intensities of the 1515 and 1430 cm^{-1} bands using a peak-fitting program that fits the sample spectrum with a straight line, a devolatilized spectrum, a pure 1630 cm^{-1} band for molecular H_2O, and a pure carbonate doublet (unpublished program by S. Newman). The CO_2 concentrations were then calculated using compositionally dependent absorption coefficients (Dixon and Pan, 1995) based on major element composition determined by microprobe analysis. Due to uncertainties both in inclusion thickness and in absorbance peak heights, average uncertainty at 1σ in H_2O and CO_2 concentrations is 11%. Accuracy of the FTIR technique is expected to be ±10% for H_2O and ±20% for CO_2 (Dixon, 1991).

3.2.2 EPMA

After FTIR analysis, melt inclusions were analyzed for major element composition with the Cameca SX100 electron probe at the University of Oregon. Beam conditions were as follows: 15 kV accelerating voltage, 20 nA beam current, and a beam diameter of 10 microns. Element count times were as follows: 10 sec (Mn), 20 sec (Ca, S, Cl, Ti), 30 sec (Mg, Si), 40 sec (K, Al, P), 60 sec (Fe). To minimize effects of element migration, concentrations of Na, K, and Si were corrected back to time zero using time-dependent intensity measurements. Olivine host compositions were also analyzed, at a spot located a distance of ~100 microns from both the edge of the host crystal and the inclusion. Intensities were corrected by either linear off-peak background correction (K, Mn, S, Cl, Ti and P) or the mean atomic number (MAN) background correction procedure (Na, Si, Al, Mg, Fe and Ca) of Donovan and Tingle (1996). Measured standard concentrations were within 0.07% of published values, except S, which was within

0.92% of published values. Percent standard deviation, based on replicate analyses of each inclusion, was ≤ 5% for all elements except Mn, which was ≤7%.

For the Whitechuck and Indian Pass melt inclusions, the S K_α peak position was measured using the JEOL 8500F field emission electron microprobe at Washington State University (following procedures in Carroll and Rutherford, 1988; Wallace and Carmichael, 1994). Beam conditions were as follows: 15kV accelerating voltage, 30 nA beam current, and a beam diameter of 5 microns. Count times were 5 sec for standards and 30 sec for unknowns. To avoid oxidation of sulfur during analysis, the beam position was moved 1 µm each 60 s during the analysis. Troilite and pyrrhotite standards were run before and after the glass inclusions to monitor accuracy. Pyrite and anhydrite standards were analyzed at the start and end of the run to calculate sulfur speciation (Rowe et al., 2007). Precision, based on replicate analyses, was better than 10% at 1 σ for all samples. For all other melt inclusions, we used an S K_α peak position that was intermediate between those for anhydrite and pyrite (~30% of the full shift between pyrite and anhydrite; Wallace & Carmichael, 1994).

3.2.3 LA-ICP-MS

Trace element compositions of melt inclusions were measured with a laser ablation inductively coupled mass spectrometer (VG PQ ExCell quadrupole ICP-MS and NewWave DUV 193 nm ArF Excimer laser) at Oregon State University. Beam conditions were 3 Hz, beam size was 50 µm with a 45 s total dwell time. Dwell time per element was 10 milliseconds. Glass standard GSE-1G was used for calibration and 43Ca was used as an internal standard. Accuracy at 1σ was ≤5% from accepted values. Precision was ≤5% for trace elements Ti, V, Sr, Y, Zr, Ba and Ce, ≤10% for trace elements Sc, Rb, Nb, La, Pr, Nd, Pb, ≤15% for Sm, Eu, Hf, and Th, and ≤20% for Gd, Dy, Er, Yb, Ta and U.

3.3. Post-entrapment modification corrections

Inclusions can undergo a number of potential post-entrapment compositional changes. These include post-entrapment crystallization of olivine along the melt-host interface, diffusive loss of Fe to the host olivine, diffusive loss or gain of H^+, and CO_2 transfer to a vapor bubble (e.g., Danyushevsky et al., 2000; Gaetani and Watson, 2000; Portnyagin et al., 2008; Wallace et al., 2021). Melt inclusion compositions were corrected for post-entrapment crystallization (PEC)

by adding equilibrium olivine (in steps of 0.1 wt.%) until equilibrium between host and inclusion was achieved (Danyushevsky et al., 2000). The effect of PEC on volatile and trace element concentrations was corrected by using the change in K_2O as a proxy for elements incompatible in olivine. Iron loss was corrected using Petrolog 3.1 (Danyushevsky and Plechov, 2011), assuming initial FeO^T of the inclusion are best estimated by the whole rock compositions.

Diffusive loss of H^+ can occur over short timescales (less than 2 days; e.g., Bucholz et al., 2013). For this study, we use loose olivine phenocrysts in ash-sized tephra, which likely cooled rapidly, to decrease the likelihood of diffusive loss of hydrogen during eruption and quenching (Lloyd et al., 2013). Furthermore, we compare relationships between K_2O and H_2O to assess the potential for post-entrapment diffusive loss (e.g., Lloyd et al., 2013; Johnson et al., 2020).

4. Results

4.1.1 Melt Inclusion major and trace element compositions

Melt inclusions corrected for post-entrapment crystallization from each sample display distinct major element compositions. While a majority of the melt inclusions can be defined as medium-K calc-alkaline basalts to basaltic andesites (Fig. 2), the full dataset displays a range from low-K to high-K compositions (<0.5 wt.% to >1.5 wt.% K_2O). Melt inclusions suites from individual samples are similar to or slightly less-evolved than previously published whole-rock compositions (Fig. 2).

4.1.2 Mount Saint Helens Castle Creek Basalts

Data was acquired from melt inclusions and host olivine from two MSH basaltic tephra units, Bu-2 and Bu-3. The olivine hosts from the Bu-2 tephra (Fo_{79}-Fo_{85}) have similar to slightly higher Mg than those from the Bu-3 tephra (Fo_{74}-Fo_{83}). As a result, melt inclusions from Bu-2 after correction for PEC have MgO concentrations that overlap with Bu-3 but extend to higher values (4.7 – 7.8 wt.% and 6.3 – 9.0 wt.% MgO, respectively; Supplementary Figures). Melt inclusion compositional suites from both samples also overlap with whole-rock compositions but extend to more mafic compositions along trajectories consistent with olivine fractionation. The two MSH samples primarily differ in their alkali abundances. The Bu-2 melt inclusions have moderate-K compositions whereas the Bu-3 melt inclusion suite has compositions that range from med- to high-K compositions.

301

302 *4.1.3 Indian Heaven Basalts*

303 From the Indian Heaven volcanic field, data was acquired from melt inclusions and host
304 olivine from two different basaltic units, QVTC and QVBP. The olivine phenocrysts hosting
305 melt inclusions from QVTC range from Fo_{84}-Fo_{87}. Olivine-hosts from QVBP are more evolved
306 and range from Fo_{80}–Fo_{83}. Melt inclusions (corrected for PEC) from QVTC have relatively low
307 K2O (<1 wt.%) relative to the other med-K calc-alkaline basalts analyzed in this study, while
308 those from QVBP are distinctly low-K (Fig.2). Both melt inclusion suites also display relatively
309 high MgO concentrations (QVTC = 7.25-9.64 wt.%; QVBP = 6.46 – 8.04wt.%) and are
310 consistent with previously analyzed whole rock analyses from the same geologic units and other
311 basaltic samples in the Indian Heaven region (Korosec, 1989; Supplementary Figures).

312

313 *4.1.4 Glacier Peak Basalts*

314 The PEC-corrected major element compositions for melt inclusions from Indian Pass (IP)
315 generally fall within the medium-K calc-alkaline field, whereas those from Whitechuck (WC)
316 extend from the low-K tholeiite field to the boundary between LKT and medium-K basalt (Fig.
317 2). The olivine hosts from the Indian Pass CAB are the most Mg-rich measured in this study and
318 range from Fo_{87}-$Fo_{89,}$ whereas those from the Whitechuck LKT are $Fo_{86.}$ Whole-rock analyses
319 from the same samples have similar K_2O concentrations but display elevated MgO and Al_2O_3
320 concentrations compared to the melt inclusions (Taylor, 2001; Shaw 2011).

321

322 *4.2 Magmatic Volatile Compositions*

323 The PEC-corrected melt inclusions in the WA Cascades sample suite have variable H_2O
324 concentrations that range from ~0.3–2.2 wt.% (Fig. 3). Most samples display a range of
325 relationships between other volatiles and K_2O, suggestive of differences in ascent, degassing,
326 and crystallization histories.

327 Comparatively alkali-rich samples from Mount St. Helens have H_2O concentrations that
328 range from 0.32–1.94 wt.%. Both samples display a positive correlation between Cl and K_2O
329 indicative of Cl enrichment during fractional crystallization (Fig. 3), suggesting that Cl, which is
330 more soluble than the other volatiles, was not lost by degassing prior to melt inclusion
331 entrapment. Variation of H_2O with K_2O for Bu-2 suggests the effects of degassing induced

crystallization (e.g., Johnson et al., 2008), whereas degassing related loss is smaller for Bu-2. The behavior of S is somewhat between that of H2O and Cl, with some inclusions showing increases due to fractional crystallization and others showing small to moderate losses.

From Indian Heaven, melt inclusions from the low-K sample, QVBP, display little to no variation in volatiles or major elements (Figs. 2 and 3). However, relatively high S concentrations (>900 ppm) suggest that these samples are not significantly degassed. Conversely, melt inclusions from the CAB sample (QVTC) show relationships between H_2O, S, Cl, and K_2O that are indicative of S and H_2O degassing and residual enrichment of Cl during degassing induced crystallization.

From Glacier Peak, Whitechuck (LKT) melt inclusions have a large range in H_2O concentration (0.5-2.0 wt.%) that does not correlate with K_2O (Fig. 3), Cl, or S. Given the homogeneity of S and Cl values, we suggest the variable H_2O is caused by post-entrapment diffusive loss, likely during ascent. Corrected Indian Pass (CAB) melt inclusions have H_2O contents that range from 1.1-2.2 wt.%. Similar to the QVBP sample Indian Heaven, this melt inclusion suite shows relationships between H_2O, S, Cl, and K_2O that are suggestive of S and H_2O degassing, and enrichment of Cl during degassing induced crystallization. These melt inclusions are also notable for their relatively high S concentrations (2550-3320 ppm).

4.3 Parental melt compositions

While melt inclusions hosted in high-Fo olivine record the most primitive melts accessible for analysis, they typically do not have compositions in equilibrium with their initial mantle source peridotite (olivine Fo≥90). Therefore, further corrections are made to estimate the compositions of the parental melts of these primitive magmas. The simplest assumption is that the primary mantle-derived melts fractionated olivine only before being trapped as melt inclusions. Thus, for each melt inclusion suite, a primary melt composition was calculated by taking an average of the most MgO- and H_2O-rich melt inclusions and incrementally adding olivine until the composition reached equilibrium with Fo_{90}. Concentrations of trace elements and volatile elements that are incompatible in the olivine hosts were corrected assuming similar behavior to K_2O during olivine-only fractionation (percentages found in Supplementary Tables).

The resultant Fo_{90} equilibrium compositions provide more robust comparisons of inferred mantle source regions for magmas in this study to other arcs, MORBS and OIBS. A comparison

of the Fo_{90} equilibrium Cl/K_2O values from all WA Cascades samples generally overlap with those measured in mafic magmas from the Lassen and Central Oregon regions of the Cascade Arc (Fig. 4). While the maximum H_2O in the Fo_{90} equilibrium compositions overlap with those calculated from the Garibaldi Belt melt inclusions (Venugopal et al., 2020), they fall at the lower end of the range (or below for Indian Heaven LKT) of Lassen and Central Oregon, all of which have numerous samples with H_2O concentrations >2.5 wt.% H_2O.

5. Discussion

5.1 Distinguishing Mantle Sources in WA Cascades Magmas

Quantification of slab contributions to arc magmas requires an understanding of the mantle source composition to which various slab components have been added. Numerous studies of high-MgO Cascade Arc magmas have identified several distinct compositional types, the most widespread of which are LKT, CAB, and OIB types (e.g., Schmidt et al., 2008). These types have been interpreted as being derived by melting of compositionally distinct mantle source regions (Leeman et al., 1990; Bacon et al., 1997). These components are variably distributed along the length of the arc, although there is a higher abundance of the OIB-type in the northern Oregon and southern Washington regions (Pitcher and Kent, 2019). At Mount St Helens alone it is suggested that all three magma types are present: hydrous arc basalt produced by flux melting, LKTs interpreted as decompression melts from the upper mantle, and HFSE-rich basalts (IPB or OIB) derived from a water-poor and incompatible-trace-element-rich source (Wanke et al., 2019). Thus, outstanding questions remain about the scale of mantle heterogeneity in the Cascades.

Concentrations of Nb are commonly used to investigate mantle processes because it is not fluid mobile during slab dehydration and is highly incompatible during mantle melting. Figure 5 shows the concentrations of Zr, a high field strength element (HFSE), Ce, a representative light rare earth element (LREE), Ba, a representative large ion lithophile element (LILE) and K_2O, a relatively incompatible major element in basalts, with respect to Nb for all melt inclusions, whole-rock analyses from the literature, and Fo_{90}-corrected parental magma compositions. Positive relationships between all of these elements are expected due to their incompatibility during mantle melting or subsequent fractional crystallization. However, the extreme variability in Figure 5 requires considerable variation in the enriched to depleted

character of mantle sources beneath the different regions. Concentrations of Ce, Ba, and K_2O in the Glacier Peak IP (CAB) sample show enrichments compared to the positive trend of the other samples, and this likely results from addition of a slab-derived component (Fig. 5). The variation between samples importantly highlights that all samples investigated in this study, even those from the same volcanic centers, show indications of heterogeneous mantle source compositions, which need to be carefully considered when trying to decipher volatile and trace element contributions from subducted lithologies. In particular, the moderate- to high-K character of most samples on the K_2O vs. SiO_2 diagram (Fig. 2) appears to be the result of enriched mantle sources (compare Fig. 4d), with only the Glacier Peak IP CAB sample having elevated K_2O because of a slab contribution.

Trace element ratios, such as Nb/Zr and Dy/Yb, also provide evidence that most of the variability between samples in this study is likely related to differences in mantle source compositions (Fig. 5). Comparisons of WA Cascades parental magma compositions to MORB, OIBs, and arcs globally further highlights their globally impressive variability. While all samples overlap with the global arc array from Ruscitto et al. (2012), Mount St. Helens samples (Bu-2 and Bu-3) have relatively high Nb/Y compositions similar to many OIB globally, in keeping with their alkalic major element compositions and high HFSE concentrations (Wanke et al., 2019). In contrast, both LKT samples from Indian Heaven (QVBP) and Glacier Peak (WC) have similarly depleted Nb/Y ratios and overlap with N-MORB. The CAB samples, QVTC from Indian Heaven and Glacier Peak IP, have intermediate Nb/Y ratios that overlap with enriched MORB and depleted OIB (Fig. 6).

Interestingly, each volcanic center displays more than one of these mantle components, which suggests that mantle heterogeneity is present at the volcano-scale. In the southern WA Cascades in the vicinity of Mount St Helens and Indian Heaven volcanic field, the presence of a "slab gap" interpreted from seismic tomography has been suggested to provide a pathway for more enriched asthenospheric mantle upwelling and to explain why volcanic centers are offset tens of km west from the main volcanic front (Hildreth, 2007; Schmandt and Humphreys, 2010; Mullen et al., 2017; Hawley and Allen, 2019; Wanke et a., 2019). This mechanism may provide an explanation for the presence of OIB-like magmas (with likely garnet-influenced Dy/Yb – see Fig. 6) in this region, despite the predominance of an isotopically homogeneous MORB-type depleted mantle beneath much of western North America (Mullen et al., 2017). However, a

recent study using seismic wave amplitudes (Pang et al., 2023) shows no indication of such a hole or discontinuity in the slab beneath the WA Cascades and suggests that the Juan de Fuca slab may be continuous from Canada to northern California. Regardless, the array of mantle source heterogeneity sampled by WA Cascade magmas adds to the growing body of evidence that mantle source regions beneath arcs globally may be more variable than previously recognized and can explain some differences in primitive basalt compositions (e.g., Turner and Langmuir, 2022).

5.2 Volatile abundances in Washington Cascade magmas

Given the significant mantle source variability indicated by incompatible trace elements in WA Cascades parental magmas, we compare volatile abundances by evaluating H_2O, Cl, and S relative to Nb (Fig. 7). Concentrations of Nb (and trace element ratios including Nb) are often used to represent the relative fertility of the mantle source (i.e., enriched vs. depleted character) because Nb is highly incompatible and depleted during partial melting of the mantle (Pearce and Peate, 1995). However, previous work in the southern Cascades suggests that partial melting of the slab contributes to the subduction component (Walowski et al., 2016), in which case, experiments suggest that Nb might have a higher concentration in the slab component than it would in a fluid released by dehydration (Kessel et al., 2005). However, given the large range in Nb concentrations in the WA Cascades magmas, the relatively small amounts of slab melt or fluid added to the mantle wedge (see discussion below and Walowski et al., 2016), and the likely small magnitude of the hydrous melt-residual solid or fluid-solid partition coefficients during slab melting when rutile is present (Kessel et al., 2005), overall contribution of Nb to the mantle source is likely very minor. For this reason we consider Nb as a good indicator of the enriched to depleted character of mantle wedge sources beneath the WA Cascades before addition of any slab components.

To examine the addition of volatile elements from the slab component, we compare our results to the MORB array at a given Nb concentration (Fig. 7). The results suggest that the elevated H_2O and Cl in Mount St. Helens basalts (Bu-2 and Bu-3) compared to uncontaminated MORB is caused by addition of a small amount of a slab component. The LKT from Indian Heaven (QVBP) has the lowest H_2O of any sample in the Cascade Arc compilation and the global arc compilation from Ruscitto et al. (2012). The MORB-like values and a lack of evidence

for volatile-loss due to degassing (see Fig. 3 and Section 4.2) suggest that it represents a partial melt of a depleted mantle source with little to no subduction component. In contrast, the LKT from Glacier Peak (WC) has the lowest Nb concentration, indicative of an even more depleted source than the Indian Heaven LKT (QVBP), but it has higher H_2O and Cl concentrations indicative of volatile contributions from a slab component. Similarly, the CABs from Glacier Peak and Indian Heaven have elevated H_2O and Cl relative to the MORB array. We conclude that despite having H_2O and Cl concentrations at the lower end of the range for Cascades parental melts, all three volcanic regions have primitive melts with some contribution of slab-derived volatiles. The only exception is the LKT from Indian Heaven, which has H_2O and Cl concentrations similar to MORB. However, the WA Cascade magmas from all three volcanic centers in this study have H_2O and Cl contributions from the downgoing plate that overlap with other Cascades arc segments (e.g., central Oregon and northern California), although none extend to the highest values measured in the Cascades and arc magmas globally.

5.3 The source of volatiles in WA Cascade magmas

The inferred contributions of H_2O and Cl from subducted materials in WA Cascades magmas invites questions about the source of these volatiles and their role in magma generation beneath the Cascades. Are they derived from hydrous fluids or partial melts of slab lithologies (sediments and oceanic crust), or both?

To better understand thermal conditions at the slab-wedge interface beneath the Cascades, we use 2-D steady-state thermal models (following methods of Wada and Wang, 2009) for four transects: one extending beneath the Mt. Baker-Glacier Peak region, one beneath Mount St. Helens and Indian Heaven, one beneath the central Oregon Cascades, and one beneath the Lassen Region (Fig. 8; map locations in Fig. 1; Text S1; Figures S1-S4). In these models, the maximum depth of slab-mantle decoupling (MDD) controls the trench-ward extent of solid mantle wedge flow, and this depth tends to be 70-80 km for most subduction zones (Wada and Wang, 2009). However, slab depths beneath the Cascade arc are shallower than for many subduction zones worldwide, with estimated slab top depths of ~60 km (Mount St. Helens), ~70 km (Indian Heaven), ~90 km (Glacier Peak), 70-80 km (central Oregon Cascades), and ~90 km (Lassen; depths from McCrory et al., 2012). Temporal changes in regional tectonics or slab geometry may cause deviation from the common MDD. To show these uncertainties, we

developed models with an MDD of 75 km and 65 km for each transect. Additionally, given that the slab beneath the arc may be older than assumed in the steady state model, we developed another set of models with an MDD of 75 in which the slab at the trench is ~3 Ma older than the other two sets of models. (Figure 8; Text S1). Our thermal models do not include the effects of fluid circulation within the oceanic crust at shallow depths in the subduction zone or the latent heat of fusion that would affect temperatures if the oceanic crust at the plate top was partially melted. Each of these effects could reduce the slab surface temperatures by ~50 °C (Cozzens et al., 2012). Calculated slab surface temperatures beneath the Mt. Baker-Glacier Peak region, Indian Heaven, central Oregon Cascades (Three Sisters), and the Lassen Region are above the solidi of MORB+H_2O (Schmidt and Poli, 1998; Sisson and Kelemen, 2018), indicating the likelihood of partial melting of the slab top if H_2O is present (Fig. 8). This is consistent with observations in the Lassen segment of the Cascades where both geochemical observations and geodynamic models provide evidence of slab surface temperatures above the wet eclogite solidus at sub-arc depths (Walowski et al., 2015). The resulting hydrous partial melts of the subducted oceanic crust, which are expected to be dacitic in composition (Klimm et al., 2008) would drive partial melting of mantle wedge peridotite to produce hydrous basalts with unique, albeit subtle, geochemical fingerprints (Walowski et al., 2015; 2016). However, because Mount St. Helens is much closer to the trench than other Cascade volcanoes, the estimated range of slab surface temperatures are both below and above the MORB+H_2O (Fig. 8b). This suggests that hydrous slab melting may not occur beneath Mount St. Helens, assuming vertical transport of fluids and melts through the mantle beneath the edifice. This is consistent with seismic studies suggesting the mantle wedge just to the west of Mount St. Helens is relatively cold and dry (Pang et al., 2023). Furthermore, a seismic low-velocity anomaly at 15-30 km depth extending SE from beneath Mount St. Helens to beneath Mt. Hood is interpreted as a deep crustal magma reservoir, suggesting that magmas feeding Mount St. Helens are ultimately derived from the mantle wedge further to the east (Jiang et al., 2023).

To determine the effect of slab melt addition to the mantle wedge, we use a similar method as Walowski et al. (2016) to quantify the effects of hydrous melt addition to peridotite (Fig. 9). To do this, we created mantle-wedge source compositions by adding various amounts of a 5% partial melt of Gorda MORB (Davis et al., 2008) to two different mantle compositions. Trace element concentrations in a partial melt of MORB was calculated using partition

coefficients for a rutile-bearing eclogite at sub-arc depths (Sisson and Kelemen, 2018). We mixed 2, 5, and 10% of this partial melt with both a depleted MORB mantle composition (Salters and Stracke, 2005) and a primitive mantle composition (Sun and McDonough, 1989). The mixtures were then partially melted by 5, 10, 15, and 20%, consistent with the degrees of partial melting expected in the mantle wedge beneath the Cascades (Figure 9a and b; e.g., Walowski et al., 2016). Although we did not attempt to model the kind of reactive transport mechanism that likely occurs in the mantle wedge, our approach is conceptually similar to that used by experimental petrologists to simulate mantle melting (e.g., Grove et al, 2002), which involves equilibration of a given bulk composition at various temperatures and pressures. Figure 9A shows how most WA Cascades magmas have Sr/Y ratios similar to the southern and central Cascade magmas, consistent with a slab component that includes a partial melt of garnet-bearing eclogite.

Recent experimental work by Rustioni et al. (2021) suggests that much of the trace element variability in subduction zone magmas can be explained by differences in the salinity of slab fluids. Their study investigated partitioning of major and trace elements between eclogite (with and without rutile) and aqueous fluids with variable salinity. The experiments indicate that large ion lithophile elements (LILE), light rare earths (LREE), Pb, and U have partition coefficients that increase with increasing salinity, whereas typical high field strength elements, such as Ti, Nb, and Ta, and HREE are not mobilized even at high salinities. Figure 9 C and D also compares WA Cascade melt inclusion compositions to predicted trace element compositions of mantle melts with an added subduction component of variable salinity (1-7%) in equilibrium with both rutile-bearing and rutile-free eclogites, calculated using the "subduction calculator" of Rustioni et al. (2021). Most Cascade Fo_{90} equilibrium compositions have Sr/Y ratios consistent with 5-20% partial melts of a depleted mantle or primitive mantle source to which moderate amounts of a low salinity fluid have been added (Fig. 9a). However, fluid amount and salinity alone cannot explain the highest Sr/Y values. Specifically, slab melt addition is likely required to explain the highest Sr/Y ratios from the Lassen Region and the Glacier Peak CAB. This provides further support that slab melting may not be restricted to the southern Cascades (Walowski et al., 2016; Mullen et al., 2017; Sas et al., 2017). Taken together, for most Cascade melt inclusion compositions, the increase of Cl in fluids results in trace element enrichments that cannot be distinguished from partial slab melts. However, the high slab surface temperatures predicted by

geodynamic models (Figure 8) suggest hydrous partial slab melting is possible beneath all Cascade arc segments, and both processes may contribute to magma petrogenesis as they are not mutually exclusive.

Because Nb is used here as an important indicator of mantle enrichment, it is important to test how it is affected by subduction component addition. Figure 9b and d show variability in Ba/Nb relative to Nb. Similar to Sr/Y values in figure 9a, most Cascades Arc magmas have Ba/Nb ratios that can either be explained by either hydrous fluids and/or a partial slab melt added to mantle wedge peridotite. However, the model results highlight that variability in Nb is dominantly driven by mantle source composition (enriched vs. depleted) and degree of partial melting. The OIB-type magmas at Mount Saint Helens have the highest Nb concentrations amongst the Cascade arc melt inclusion datasets, which requires a mantle component that is significantly more enriched than primitive mantle or a very small degree of melting (<2%). Although slab eclogite melt addition can lead to ~7 ppm increases in Nb concentrations when added to a primitive mantle composition, the Mount Saint Helens magmas have Nb concentrations that would require a mantle component with even higher Nb. This is consistent with their alkali-rich major element and previously published radiogenic isotope compositions (Wanke et al., 2019).

We also compare Th/Yb ratios, which are commonly used as tracers of contributions from a sediment component, to Nb/Yb, which indicates the enriched to depleted character of the mantle wedge, which in turn is largely controlled by extent of previous melting and melt extraction and/or refertilization by mantle melts (Figure 10a; Pearce and Peate, 1995; Iveson et al., 2021). Assuming that the MORB array, which shows a strong correlation between Nb/Yb and Th/Yb, represents a baseline with no slab contributions, the relative enrichment of Th/Yb from this array should represent the relative contribution of various subduction components (Figure 10a). Consistent with the results from Figures 5 and 6, Mount St. Helens basalts (Bu-2 and Bu-3) are derived from a mantle source that is very enriched based on Nb/Yb. However, despite having some of the highest Th/Yb values in the WA Cascades dataset presented here, relatively modest deviation from the MORB array indicates that these samples have only a modest amount of a slab component added to their mantle source, similar to most Cascade CABs and LKTs. The CAB from Glacier Peak has a similar Nb/Yb value to the CAB from Indian

Heaven, but the CAB from Glacier Peak has a Th/Yb ratio that is a three times higher. This likely indicates that the Glacier Peak sample has a larger proportion of a subduction component.

Unlike Sr/Y and Ba/Nb (Figure 9), the Th/Yb ratios for the Glacier Peak CAB and some Lassen region magmas cannot be explained by slab melt addition or slab fluid salinity. Rather, the data trend toward bulk north Cascadia offshore sediment compositions. This is consistent with Mullen et al. (2017), who found that Glacier Peak CABs overlap with the least radiogenic High Cascades data in $^{208}Pb/^{204}Pb$ vs. Hf/Pb space and therefore record a relatively sediment-dominated bulk subduction component, unique to this region of the Cascades. In contrast, southern WA Cascade samples from Mount St. Helens and Indian Heaven display lower amounts of slab contributions that are best explained by either hydrous slab melts or variably saline fluids added to a mantle peridotite. Interestingly, the unusually high Th/Yb sediment signature is also seen in magmas from the Lassen region but not from central Oregon. Beneath the forearc region of northern WA and northern CA, seismic data indicates the presence of thick (~10 km), anomalously low shear-wave velocity zones that are interpreted to be "subcreted" metasedimentary material that has been emplaced through successive subcretion events over geologic timescales (Delph et al., 2021). Such material is not present beneath the forearc in southern WA and Oregon because the thick, accreted Siletzia crust forms a backstop extending all the way to the plate interface, preventing deeper sediment subduction. The Th/Yb data suggests that beneath the far northern WA and northern California (Lassen) segments of the arc, some of the thick metasedimentary material is more deeply subducted and entrained back into the mantle, where it can contribute to mantle melting (Hacker et al., 2011).

The deviations of H_2O and Cl values from the MORB array (Fig. 7) also support the hypothesis that all WA Cascades magmas, except for the Glacier Peak LKT, contain volatiles contributed by a slab component added to the mantle wedge (Fig. 10b). We show these deviations quantitatively using ΔCl and ΔH_2O, which are the vertical deviations of each of our parental melt compositions from best fit lines to the MORB arrays on Figures 7a and b. The delta parameters allow us to compare the Cl and H_2O deviations from the MORB array in a way that subtracts out the effects of variable mantle source composition. The result shows that most WA Cascade samples require a slab component with Cl/H_2O ratio similar or slightly higher than seawater, similar to the lower end of the range for central Oregon. However, the Glacier Peak

609 CAB sample requires a slab component with lower Cl/H_2O ratio, more similar to Lassen region
610 magmas, consistent with other trace element systematics (e.g., Figures 9 and 10b).
611
612 *5.4 Implications for mantle melting beneath the Cascade Arc*
613 The Cascade Arc serves as a natural laboratory to explore petrogenesis in an endmember
614 subduction zone with a hotter-than-average slab geothermal gradient (e.g., van Keken et al.,
615 2011). In the WA Cascades, low whole-rock concentrations of the highly fluid mobile element B
616 led Leeman et al. (2004; 2005) to conclude that magmas were volatile-poor and formed primarily
617 by decompression melting caused by mantle upwelling or convection. Thermobarometry
618 calculations by Leeman et al. (2005; 2020) further suggested that LKT and OIB-like magmas
619 erupted in the WA Cascades last equilibrated with mantle at conditions above the anhydrous
620 peridotite solidus, leading to the interpretation that no slab-derived fluid was involved. However,
621 the results presented here support the interpretation that WA Cascades basaltic magmas,
622 regardless of mantle fertility and type (including LKT and OIB-type), have volatile and trace
623 element compositions that point to contributions from the slab, albeit variable, from small to
624 moderate amounts. Rather than viewing arc magma generation as being wet vs. dry, the data for
625 the Cascades reinforces that melting beneath arcs reflects variations in slab inputs superimposed
626 on heterogeneous mantle compositions and further modulated by spatially variable, upwelling-
627 driven decompression (driven by corner flow, small-scale 3D convection, and/or flow through a
628 slab tear). The relative roles of mantle temperature and H_2O addition (either as fluids or hydrous
629 melts) in driving melting can be shown quantitatively using the relations in Portnyagin et al.
630 (2007). Given low to moderate inputs of slab-derived H_2O beneath many regions of the
631 Cascades, high mantle temperatures and decompression melting are important for driving partial
632 melting, especially for the refractory mantle source regions of LKT.
633
634 **6. Conclusions**
635 From this investigation of volatile (H_2O, S, and Cl), major, and trace element
636 compositions of olivine-hosted melt inclusions in relatively primitive basalts (> 6 wt.% MgO)
637 from three volcanic centers in the Washington Cascades (Glacier Peak, Indian Heaven, and
638 Mount St. Helens) we conclude that:

(1) The Washington Cascades sub-arc mantle is remarkably heterogeneous. Trace element ratios span nearly the entire range of arc magmas globally, from high Nb/Zr and OIB-like compositions at Mount St. Helens, to LKTs from Indian Heaven and Glacier Peak that have N-MORB-like Nb/Zr. These mantle heterogeneities are present from the volcano-scale to the arc-scale and highlight the importance of constraining mantle heterogeneity when interpreting slab contributions.

(2) Volatile contributions from the slab are identifiable across the spectrum of different magma types (LKT, CAB, and OIB) present in the WA Cascades. We observe small to moderate H_2O and Cl contributions from the downgoing slab regardless of mantle fertility or depletion.

Additionally, comparison of data with other Cascade arc segments, previous geochemical studies, comparison to experimentally-derived slab component calculators, and comparisons with geodynamic model, we conclude that both fluid salinity variability and partial slab melting, non-uniquely, may contribute to subduction component trace element characteristics of magmas along the entire Cascade Arc. We also find individuality at volcanic centers along the WA Cascades. Mt. Saint Helens magmas have trace element compositions consistent with an enriched mantle source region, although the origins of this enrichment remain unresolved. Despite their proximity to Mount Saint Helens, Indian Heaven magmas are derived from some of the most depleted mantle source regions, and the LKT sample has very low primary H_2O content and no indication of a slab melt component. Glacier Peak magmas are from similarly depleted mantle source regions as the Indian Heaven Volcanic field but have unique subduction components with high Th/Yb, likely bulk sediment related. These high Th/Yb ratios are similar to those found in the Lassen region and may be explained by “subcreted” metasedimentary material, north and south of the boundaries of the Siletzia Terrane. These signatures are not present in the central Oregon and southern Washington Cascades which overly the Siltzia Terrane and may block subcretion of this material in the central portions of the arc. Taken together, the results provide evidence for a complex and important role for materials contributed by the subducting slab in the petrogenesis of magmas beneath the Cascade arc.

Acknowledgements

We thank Adam Kent for assistance with LA-ICP-MS measurements, John Donovan for assistance with EPMA, and Mike Clynne for assistance in the field with sample collection. We appreciate the constructive reviews of [TBD] and assistance from the editor [TBD]. Funding was provided by the National Science Foundation (EAR-1119224 and EAR-1019848).

Supplementary Data Tables

Table S1: Primary melt compositions; highest MgO melt inclusions from each suite calculated to be in equilibrium with Fo_{90} olivine using MiMIC (Rasmussen et al., 2020).

Table S2: Post-entrapment corrected melt inclusion compositions

Table S3: Petrologic modelling parameters; starting mantle compositions and partition coefficients

Table S4: Uncorrected major and trace element data for Glacier Peak melt inclusions and host olivine from Shaw (2011)

Table S5: Uncorrected major and trace element data for MSH and Indian Heaven melt inclusions and host olivine

Supplementary Text: Explanation of geodynamic modeling methods and parameters

Data Availability Statement

The data presented in this study and used model parameters are included in the Supplementary Data Tables and will be made available in the online Zenodo open repository prior to the publication of the manuscript. Measured and uncorrected melt inclusion data for Glacier Peak is already freely available in Western Washington University's repository, CEDAR, within Shaw (2011) https://doi.org/10.25710/6zmb-5625.

Code availability statement

The code used to generate the thermal models can be accessed by contacting I. Wada, as the use of the code requires training.

Figure Captions

Figure 1:

Regional map of the Northwestern United States showing major tectonic boundaries. The Cascade volcanic arc is defined by the major peaks (black triangles). Black arrows show convergence direction and are labeled with the convergence rate relative to North America. Sample localities interrogated in this study are highlighted by larger symbols with colors used in subsequent figures. Dashed orange lines represent locations of 2-D thermal models presented in figure 8.

Figure 2:

The SiO_2 (wt.%) vs. K_2O (wt.%) for all samples analyzed in this study. Open symbols represent previously published bulk rock analyses (Korosec, 1989; Taylor, 2001; Clynne et al., 2008; Wanke et al., 2019). Small, filled symbols represent individual melt inclusion compositions corrected for post-entrapment crystallization. Large symbols represent a Fo_{90} equilibrium composition determined for the suite of melt inclusions (see Section 4.2 in text). Low-K, Calc-alkaline, and high-K fields as defined by Gill, (1981).

Figure 3: The K_2O (wt.%) vs. H_2O (wt.%), S (ppm), and Cl (ppm) for all samples analyzed in this study. Small, filled symbols represent individual melt inclusion compositions corrected for post-entrapment crystallization. Large symbols represent a Fo_{90} equilibrium composition determined for the suite of melt inclusions (see Section 4.2 in text). Note the difference in y-axis scale for each center.

Figure 4:

The Cl/K_2O (wt.%) vs. H_2O (wt.%) for all samples analyzed in this study. Small, filled symbols represent individual melt inclusion compositions corrected for post-entrapment crystallization. Large symbols represent a maximum H_2O and Fo_{90} equilibrium composition determined for the suite of melt inclusions (see Section 4.2 in text). Data from Central Oregon, Lassen region, and Garibaldi belt also represent Fo_{90} equilibrium compositions calculated from a suite of melt inclusions (Ruscitto et al., 2010; Walowski et al., 2016; Venugopal et al., 2020).

Figure 5:

The Nb ppm vs. A) Zr ppm, B) Ce ppm, C) Ba ppm, and D) K_2O (wt.%) for all samples analyzed in this study. Open symbols represent previously published bulk rock analyses (REFS). Small filled symbols represent individual melt inclusion compositions corrected for post-entrapment crystallization. Large symbols represent a Fo_{90} equilibrium composition determined for the suite of melt inclusions (see Section 4.2 in text).

Figure 6:

The Dy/Yb vs. Nb/Zr for all samples analyzed in this study compared to global compilations of MORB (Gale et al., 2014; LeVoyer et al., 2019), OIB (GEOROC Database compilation, Lehnert et al., 2000), and arc basaltic primary melts based on melt inclusions (Ruscitto et al., 2012). Large symbols represent a Fo_{90} equilibrium composition determined for the suite of melt inclusions (see Section 4.2 in text).

Figure 7:

The Nb ppm vs A) H_2O, B) Cl, and C) S for all samples analyzed in this study compared to global compilations of MORB (small blue diamonds; LeVoyer et al., 2019) and arc basalts (small grey circles; Ruscitto et al., 2012). Large colored symbols represent a Fo_{90} equilibrium composition determined for the suite of melt inclusions (see Section 4.2 in text). Data from Central Oregon and Lassen regions also represent Fo_{90} equilibrium compositions calculated from a suite of melt inclusions (Ruscitto et al., 2010; Walowski et al., 2016).

Figure 8: Slab surface temperature with increasing depth predicted by 2-D geodynamic models for the a) Glacier Peak - Mount Baker region, b) Mount St. Helens region, c) central Oregon region (Three Sisters) and d) the Lassen region. Heat flow suggests the best estimate for slab temperatures are for MDD of 75 km (red solid line), but uncertainty is captured by additional models that show a slab that is ~3 Ma younger at the trench (dashed blue lines) and one with an MDD of 65 (purple dashed lines). Two MORB + H_2O solidi are from Schmidt and Poli (1998) and Sisson and Kelemen (2018). Grey bars show the approximate depth of the slab beneath main

761 volcanic edifices for each segment based on the slab geometry of McCrory et al. (2012). See text
762 and Supplementary Text for model details.
763
764 **Figure 9:** The Y vs. Sr/Y (panels a and c) and Nb vs. Ba/Nb (panels b and d) for all samples
765 analyzed in this study compared to global compilations of MORB (LeVoyer et al., 2019). Large
766 colored symbols represent a Fo_{90} equilibrium composition determined for the suite of melt
767 inclusions (see Section 4.2 in text). Data from Central Oregon and Lassen regions also represent
768 Fo_{90} equilibrium compositions calculated from a suite of melt inclusions (Ruscitto et al., 2010;
769 Walowski et al., 2016). Panels a) and b) have black and grey solid lines that represent partial
770 melts of either DMM or PM to which partial melts of a rutile-bearing eclogite at sub-arc depths
771 were added. Each line represents partial melt fractions from 5-20% (labeled in panel A), high to
772 low Nb, respectively, in panel b) of each mixture (see section 5.3 in text for additional details).
773 Panels c) and d) show the same data with red dashed modelled curves that represent results of a
774 partial melting model developed by Rustioni et al., (2021) in which brines with variable Cl
775 content (from 1 to 7%, as labeled on the figure) from slabs with and without rutile are added to
776 DMM or PM at 4 GPa to the mantle wedge and the resulting fluxed wedge is partially melted.
777 For each model, we varied percent rutile in the eclogite (X), percent fluid added (Y), and mantle
778 melt fraction (Z) of either DMM (Salters and Stracke, 2005) or PM (Sun and McDonough, 1989)
779 denoted as [X,Y, Z, DMM/PM] in the following: In panel c) percent rutile produces overlapping
780 results such that Model 1 is [0 and 2, 10, 20, DMM], Model 2 is [0 and 2, 10, 20, PM], Model 3
781 is [0 and 2, 5, 10, DMM], Model 4 is [0 and 2, 5, 10, PM], Model 5 is [0 and 2, 5, 2, PM]. In
782 panel d) Model 1A is [0, 10, 20, DMM], Model 1B is [2, 10, 20, DMM], Model 3 is [2, 5, 10,
783 DMM], Model 4A is [0, 5, 10, PM], Model 4B is [2, 5, 10, PM], and Model 5 is [0, 5, 2, PM].
784
785 **Figure 10:**
786 The Nb/Yb vs. Th/Yb (panel a; Pearce and Pete 1995; Iveson et al., 2021) for all samples
787 analyzed in this study compared to MORB (LeVoyer et al. 2019). Large colored symbols
788 represent a Fo_{90} equilibrium composition determined for the suite of melt inclusions (see Section
789 4.2 in text). Data from Central Oregon and Lassen regions also represent Fo_{90} equilibrium
790 compositions calculated from a suite of melt inclusions (Ruscitto et al., 2010; Walowski et al.,
791 2016). Model results as in Figure 9 for slab fluid addition and partial eclogite melt addition to

DMM and PM mantle compositions. Panel b) shows the ΔH_2O vs. ΔCl for all samples analyzed in this study compared to global compilations of MORB (small blue diamonds; LeVoyer et al., 2019). Large colored symbols represent a Fo_{90} equilibrium composition determined for the suite of melt inclusions (see Section 4.2 in text). Data from Central Oregon and Lassen regions also represent Fo_{90} equilibrium compositions calculated from a suite of melt inclusions (Ruscitto et al., 2010; Walowski et al., 2016). Delta values for H_2O and Cl are calculated by subtracting individual Fo_{90} melt inclusion compositions from an average MORB value at a given Nb (where average MORB is calculated based on a best fit linear regression of a MORB array of LeVoyer et al. (2019) in Cl vs. Nb and H_2O vs. Nb space, respectively)

References

Anderson, A. T. (1974). Evidence for a picritic, volatile-rich magma beneath Mt. Shasta, California. *Journal of Petrology*, *15*(2), 243-267.

Bacon, C. R., Bruggman, P. E., Christiansen, R. L., Clynne, M. A., Donnelly-Nolan, J. M., & Hildreth, W. (1997). Primitive magmas at five Cascades volcanic fields: melts from hot, heterogeneous sub-arc mantle. *Canadian Mineralogist*, 35, 397-424.

Bézos, A., Escrig, S., Langmuir, C. H., Michael, P. J., & Asimow, P. D. (2009). Origins of chemical diversity of back-arc basin basalts: A segment-scale study of the Eastern Lau Spreading Center. *Journal of Geophysical Research: Solid Earth*, *114*(B6).

Blundy, J., and Cashman, K. (2005). Rapid decompression-driven crystallization recorded by melt inclusions from Mount St. Helens volcano. *Geology*, *33*(10), 793-796.

Borg, L. E., Clynne, M. A., & Bullen, T. D. (1997). The variable role of slab-derived fluids in the generation of a suite of primitive calc-alkaline lavas from the southernmost Cascades, Calilornia. *Canadian Mineralogist*, 35, 425-452.

Brown, E.H. (1987), Structural geology and accretionary history of the Northwest Cascades system, Washington and British Columbia. *Geological Society of America Bulletin*, v. 99, p. 201-214.

Bucholz, C. E., Gaetani, G. A., Behn, M. D., & Shimizu, N. (2013). Post-entrapment modification of volatiles and oxygen fugacity in olivine-hosted melt inclusions. *Earth and Planetary Science Letters*, 374, 145-155.

Carpentier, M., Weis, D., & Chauvel, C. (2013). Large U loss during weathering of upper continental crust: the sedimentary record. *Chemical Geology*, *340*, 91-104.

Carroll, M.K., and Rutherford, M.J. (1988). Sulfur speciation in hydrous experimental

glasses of varying oxidation state--results from measured wavelength shifts of sulfur X-rays. *American Mineralogist,* v. 73, p. 845-9.

Class, C., Miller, D. M., Goldstein, S. L., & Langmuir, C. H. (2000). Distinguishing melt and fluid subduction components in Umnak Volcanics, Aleutian Arc. *Geochemistry, Geophysics, Geosystems*, *1*(6).

Clynne, M. A., & Muffler, L. J. P. (2010). Geologic map of Lassen Volcanic National Park and vicinity, California. US Department of the Interior, US Geological Survey.

Conrey, R.M., Sherrod, D.R., Hooper, P.R., and Swanson, D.A. (1997). Diverse primitive magmas in the Cascade arc, northern Oregon and southern Washington. *Canadian Mineralogist,* v. 35, p. 367-396.

Cozzens, B. D., & Spinelli, G. A. A wider seismogenic zone at Cascadia due to fluid circulation in subducting oceanic crust. *Geology*, **40**, 899-902 (2012).

Danyushevsky, L. V., Della-Pasqua, F. N., & Sokolov, S. (2000). Re-equilibration of melt inclusions trapped by magnesian olivine phenocrysts from subduction-related magmas: petrological implications. *Contributions to Mineralogy and Petrology*, *138*(1), 68-83.

Danyushevsky, L. V., & Plechov, P. (2011). Petrolog3: Integrated software for modeling crystallization processes. *Geochemistry, Geophysics, Geosystems,12*(7).

Davis, A. S., Clague, D. A., Cousens, B. L., Keaten, R., & Paduan, J. B. (2008). Geochemistry of basalt from the North Gorda segment of the Gorda Ridge: Evolution toward ultraslow spreading ridge lavas due to decreasing magma supply. *Geochemistry, Geophysics, Geosystems*, *9*(4).

Dixon, J. E., & Pan, V. (1995). Determination of the molar absorptivity of dissolved carbonate in basanitic glass. *American Mineralogist*, *80*(11-12), 1339-1342.

Dixon, J.E. (1991). Degassing history of water, sulfur, and carbon in submarine lavas from Kilauea Volcano, Hawaii. *Journal of Geology, v. 99, p. 371-394.*

Elliott, T., Plank, T., Zindler, A., White, W., & Bourdon, B. (1997). Element transport from slab to volcanic front at the Mariana arc. *Journal of Geophysical Research: Solid Earth*, *102*(B7), 14991-15019.

Elliott, T. (2003). Tracers of the slab. *Geophysical Monograph-American Geophysical Union*, *138*, 23-46.

Fyfe, W.S. and McBirney, A.R. (1975). Subduction and the structure of andesitic volcanic Belts. *American Journal of Science, v. Vol. 275-A, p. 285-297.*

Gaetani, G.A. and Watson, E.B. (2000). Open system behavior of olivine-hosted melt Inclusions. *Earth and Planetary Science Letters*, v. 183, p. 27-41.

Gill, J.B. (1981), Orogenic Andesites and Plate Tectonics, *Minerals and Rocks*, Volume Volume 16: Berlin, Heidelberg, New York, Springer-Verlag.

Green, N.L., and Harry, D.L. (1999). On the relationship between subducted slab age and arc basalt petrogenesis, Cascadia subduction system, North America. *Earth and Planetary Science Letters*, v. 171, p. 367-381.

Guffanti, M., & Weaver, C. S. (1988). Distribution of late Cenozoic volcanic vents in the Cascade Range: Volcanic arc segmentation and regional tectonic considerations. *Journal of Geophysical Research: Solid Earth* (1978–2012), 93(B6), 6513-6529.

Hermann, J. & Spandler, C. J. Sediment melts at sub-arc depths: An experimental study. *Journal of Petrology*, **49**, 717-740 (2008).

Hildreth, W. (2007). Quaternary magmatism in the Cascades-geologic perspectives. *US Geological Survey professional paper*, 1744, 1-125.

Humphreys, E. D., & Grunder, A. L. (2022). Tectonic controls on the origin and segmentation of the Cascade Arc, USA. *Bulletin of Volcanology*, *84*(12), 102.

Iveson, A. A., Humphreys, M. C., Savov, I. P., De Hoog, J. C., Turner, S. J., Churikova, T. G., & Cooper, G. F. (2021). Deciphering variable mantle sources and hydrous inputs to arc magmas in Kamchatka. *Earth and Planetary Science Letters*, *562*, 116848.

Jiang, C., Schmandt, B., Abers, G. A., Kiser, E., & Miller, M. S. (2023). Segmentation and radial anisotropy of the deep crustal magmatic system beneath the cascades arc. *Geochemistry, Geophysics, Geosystems*, *24*(3), e2022GC010738.

Johnson, E. R., & Cashman, K. V. (2020). Understanding the storage conditions and fluctuating eruption style of a young monogenetic volcano: Blue Lake crater (< 3 ka), High Cascades, Oregon. *Journal of Volcanology and Geothermal Research*, *408*, 107103.

Johnson, E. R., Wallace, P. J., Cashman, K. V., Granados, H. D., & Kent, A. J. (2008). Magmatic volatile contents and degassing-induced crystallization at Volcán Jorullo, Mexico: implications for melt evolution and the plumbing systems of monogenetic volcanoes. *Earth and Planetary Science Letters*, 269(3), 478-487.

Kent, A. J., Peate, D. W., Newman, S., Stolper, E. M., & Pearce, J. A. (2002). Chlorine in submarine glasses from the Lau Basin: seawater contamination and constraints on the composition of slab-derived fluids. *Earth and Planetary Science Letters*, *202*(2), 361-377.

Kessel, R., Schmidt, M. W., Ulmer, P., & Pettke, T. (2005). Trace element signature of subduction-zone fluids, melts and supercritical liquids at 120–180 km depth. *Nature*, 437(7059), 724-727.

Korosec, M. A. (1989). *New K-Ar Age Dates, Geochemistry, and Stratigraphic Data for the Indian Heaven Quaternary Volcanic Field, South Cascade Range, Washington*. Washington Division of Geology and Earth Resources.

Le Voyer, M., Rose-Koga, E. F., Shimizu, N., Grove, T. L., & Schiano, P. (2010). Two contrasting H_2O-rich components in primary melt inclusions from Mount Shasta. *Journal of Petrology*, **51**, 1571-1595.

Le Voyer, M., Hauri, E. H., Cottrell, E., Kelley, K. A., Salters, V. J., Langmuir, C. H., ... & Füri, E. (2019). Carbon fluxes and primary magma CO2 contents along the global mid-ocean ridge system. *Geochemistry, Geophysics, Geosystems*, *20*(3), 1387-1424.

Leeman, W. P., Smith, D. R., Hildreth, W., Palacz, Z., & Rogers, N. (1990). Compositional diversity of late Cenozoic basalts in a transect across the southern Washington Cascades: implications for subduction zone magmatism. *Journal of Geophysical Research: Solid Earth (1978–2012)*, *95*(B12), 19561-19582.

Leeman, W.P., Lewis, J.F., Evarts, R.C., Conrey, R.M., and Streck, M.J. (2005a). Petrologic constraints on the thermal structure of the Cascades arc. *Journal of Volcanology & Geothermal Research*, v. 140, p. 67-105.

Leeman, W. P. (2020). Old/new subduction zone paradigms as seen from the Cascades. *Frontiers in Earth Science*, *8*, 535879.

Lloyd, A. S., Plank, T., Ruprecht, P., Hauri, E. H., & Rose, W. (2013). Volatile loss from melt inclusions in pyroclasts of differing sizes. *Contributions to Mineralogy and Petrology*, 165(1), 129-153.

McBirney, A.R. (1969). Compositional variations in Cenozoic calc-alkaline suites of Central America. *McBirney, A.R., ed., Andesite Conference, Proceedings,* Volume 65: United States, Oregon Department of Geology and Mineral Industries: Portland, OR, United States, p. 185-189.

McCrory, P. A., Blair, J. L., Waldhauser, F., & Oppenheimer, D. H. Juan de Fuca slab geometry and its relation to Wadati‐Benioff zone seismicity. *Journal of Geophysical Research: Solid Earth*, **117**, 1-16 (2012).

Mullen, E. K., & Weis, D. (2015). Evidence for trench-parallel mantle flow in the northern Cascade Arc from basalt geochemistry. *Earth and Planetary Science Letters*, *414*, 100-107.

Mullen, E. K., Weis, D., Marsh, N. B., & Martindale, M. (2017). Primitive arc magma diversity: New geochemical insights in the Cascade Arc. *Chemical Geology*, *448*, 43-70.

Mullineaux, D. R. (1996). *Pre-1980 tephra-fall deposits erupted from Mount St. Helens, Washington* (No. 1563). US Geological Survey.

Pearce, J. A., & Peate, D. W. (1995). Tectonic implications of the composition of volcanic arc magmas. *Annual review of Earth and planetary sciences*, *23*(1), 251-285.

Pitcher, B. W., & Kent, A. J. (2019). Statistics and segmentation: using big data to assess Cascades arc compositional variability. *Geochimica et cosmochimica acta*, *265*, 443-467.

Plank, T., Kelley, K. A., Zimmer, M. M., Hauri, E. H., & Wallace, P. J. (2013). Why do mafic arc magmas contain~ 4 wt% water on average? *Earth and Planetary Science Letters*, *364*, 168-179.

Portnyagin, M., Hoernle, K., Plechov, P., Mironov, N., & Khubunaya, S. (2007). Constraints on mantle melting and composition and nature of slab components in volcanic arcs from volatiles (H_2O, S, Cl, F) and trace elements in melt inclusions from the Kamchatka Arc. *Earth and Planetary Science Letters*, 255(1), 53-69.

Portnyagin, M., Almeev, R., Matveev, S., and Holtz, F. (2008). Experimental evidence for rapid water exchange between melt inclusions in olivine and host magma. *Earth and Planetary Science Letters,* v. 272, p. 541-552.

Reiners, P.W., Hammond, P.E., McKenna, J.M., and Duncan, R.A., (2000). Young basalts of the central Washington Cascades, flux melting of the mantle, and trace element signatures of primary arc magmas. *Contributions to Mineralogy and Petrology,* v. 138, p. 249-264.

Rowe, M.C., Kent, A.J.R., and Nielsen, R.L. (2007). Determination of sulfur speciation and oxidation state of olivine hosted melt inclusions. *Chemical Geology, v. 236, p. 303-322.*

Ramachandran, K., Hyndman, R. D., & Brocher, T. M. (2006). Regional P wave velocity structure of the Northern Cascadia Subduction Zone. *Journal of Geophysical Research: Solid Earth*, *111*(B12).

Ruscitto, D. M., Wallace, P. J., Johnson, E. R., Kent, A. J. R., & Bindeman, I. N. (2010). Volatile contents of mafic magmas from cinder cones in the Central Oregon High Cascades: Implications for magma formation and mantle conditions in a hot arc. *Earth and Planetary Science Letters*, 298(1), 153-161.

Ruscitto, D. M., Wallace, P. J., & Kent, A. J. R. (2011). Revisiting the compositions and volatile contents of olivine-hosted melt inclusions from the Mount Shasta region: implications for the formation of high-Mg andesites. *Contributions to Mineralogy and Petrology*, 162(1), 109-132.

Ruscitto, D. M., Wallace, P. J., Cooper, L. B., & Plank, T. (2012). Global variations in H_2O/Ce: 2. Relationships to arc magma geochemistry and volatile fluxes. *Geochemistry, Geophysics, Geosystems*, 13(3).

Salters, V.J.M., and Stracke, A. (2004). Composition of the depleted mantle. *Geochemistry,*

Geophysics, Geosystems, v. 5, p. Q05B07.

Schmidt, M. W., & Poli, S. Experimentally based water budgets for dehydrating slabs and consequences for arc magma generation. *Earth and Planetary Science Letters*, **163**, 361–379 (1998).

Schmidt, M.E., Grunder, A.L., and Rowe, M.C. (2008). Segmentation of the Cascade Arc as indicated by Sr and Nd isotopic variation among diverse primitive basalts. *Earth and Planetary Science Letters,* v. 266, p. 166-181.

Shaw, S. D. (2011). H_2O contents in olivine-hosted melt inclusions from primitive magmas in the northern Cascade arc. *Western Washington University*.

Sisson, T.W., and Grove, T.L. (1993). Experimental investigations of the role of H_2O in calc-alkaline differentiation and subduction zone magmatism: *Contributions to Mineralogy and Petrology,* v. 113, p. 143-166.

Sisson, T.W., and Layne, G.D. (1993). H_2O in basalt and basaltic andesite glass inclusions from four subduction-related volcanoes. *Earth and Planetary Science Letters, v. 117, p. 619-635.*

Smith, D. R. (1984). The petrology and geochemistry of high cascade volcanics in southern Washington: Mount Saint Helens volcano and the Indian Heaven basalt field. *Ph. D. Thesis*.

Sun, S. S., & McDonough, W. F. (1989). Chemical and isotopic systematics of oceanic basalts: implications for mantle composition and processes. *Geological Society, London, Special Publications*, *42*(1), 313-345.

Tabor, R.W., and Crowder, D.F. (1969). On batholiths and volcanoes; intrusion and eruption of late Cenozoic magmas in the Glacier Peak area, North Cascades, Washington. *United States Geological Survey,* Reston, VA, United States.

Turner, S. J., & Langmuir, C. H. (2022). An evaluation of five models of arc volcanism. *Journal of Petrology*, *63*(3), egac010.

Van Keken, P. E., Hacker, B. R., Syracuse, E. M., & Abers, G. A. (2011). Subduction factory: 4. Depth-dependent flux of H_2O from subducting slabs worldwide. *Journal of Geophysical Research: Solid Earth* (1978–2012), 116(B1).

Venugopal, S., Moune, S., Williams-Jones, G., Druitt, T., Vigouroux, N., Wilson, A., & Russell, J. K. (2020). Two distinct mantle sources beneath the Garibaldi Volcanic Belt: Insight from olivine-hosted melt inclusions. *Chemical Geology*, *532*, 119346.

Wada, I., & Wang, K. (2009) Common depth of slab-mantle decoupling: Reconciling diversity and uniformity of subduction zones. *Geochemistry Geophysics Geosystems*, 10, 1-36.

Wallace, P.J., and Carmichael, I.S.E. (1994). S speciation in submarine basaltic glasses as determined by measurements of SKalpha X-ray wavelength shifts. *American Mineralogist*, v. 79, p. 161-167.

Wallace, P. J., Plank, T., Bodnar, R. J., Gaetani, G. A., & Shea, T. (2021). Olivine-hosted melt inclusions: a microscopic perspective on a complex magmatic world. *Annual Review of Earth and Planetary Sciences*, *49*, 465-494.

Walowski, K. J., Wallace, P. J., Hauri, E. H., Wada, I., & Clynne, M. A. (2015). Slab melting beneath the Cascade Arc driven by dehydration of altered oceanic peridotite. *Nature Geoscience*, *8*(5), 404-408.

Walowski, K. J., Wallace, P. J., Clynne, M. A., Rasmussen, D. J., & Weis, D. (2016). Slab melting and magma formation beneath the southern Cascade arc. *Earth and Planetary Science Letters*, *446*, 100-112.

Wanke, M., Clynne, M. A., von Quadt, A., Vennemann, T. W., & Bachmann, O. (2019). Geochemical and petrological diversity of mafic magmas from Mount St. Helens. *Contributions to Mineralogy and Petrology*, *174*, 1-25.

Figure 1.

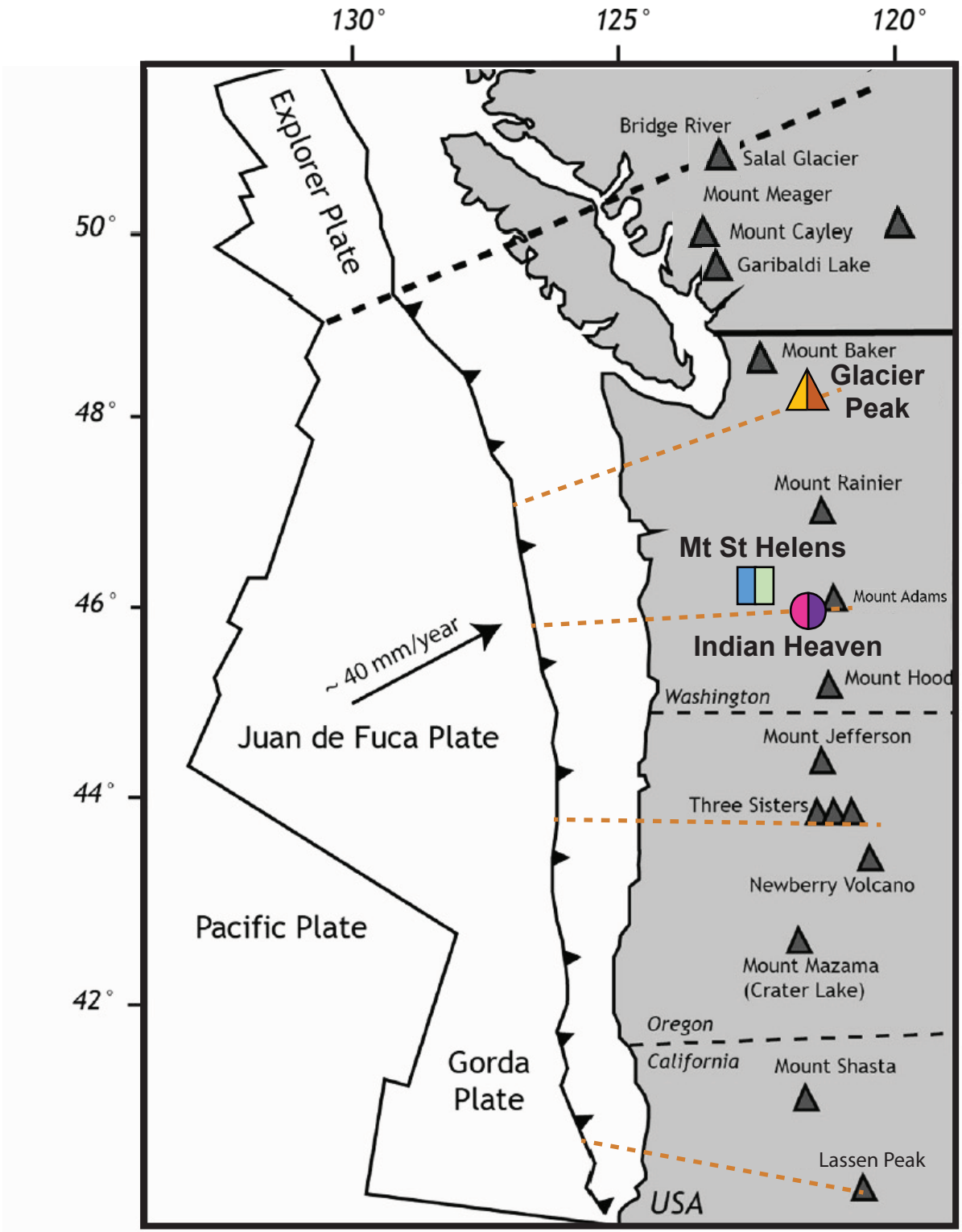
130°
125°
120°
50°
48°
46°
44°
42°
Explorer Plate
Bridge River
Salal Glacier
Mount Meager
Mount Cayley
Garibaldi Lake
Mount Baker
Glacier Peak
Mount Rainier
Mt St Helens
Mount Adams
Indian Heaven
Mount Hood
Washington
~ 40 mm/year
Juan de Fuca Plate
Mount Jefferson
Three Sisters
Newberry Volcano
Pacific Plate
Mount Mazama
(Crater Lake)
Oregon
California
Mount Shasta
Gorda Plate
Lassen Peak
USA

Figure 2.

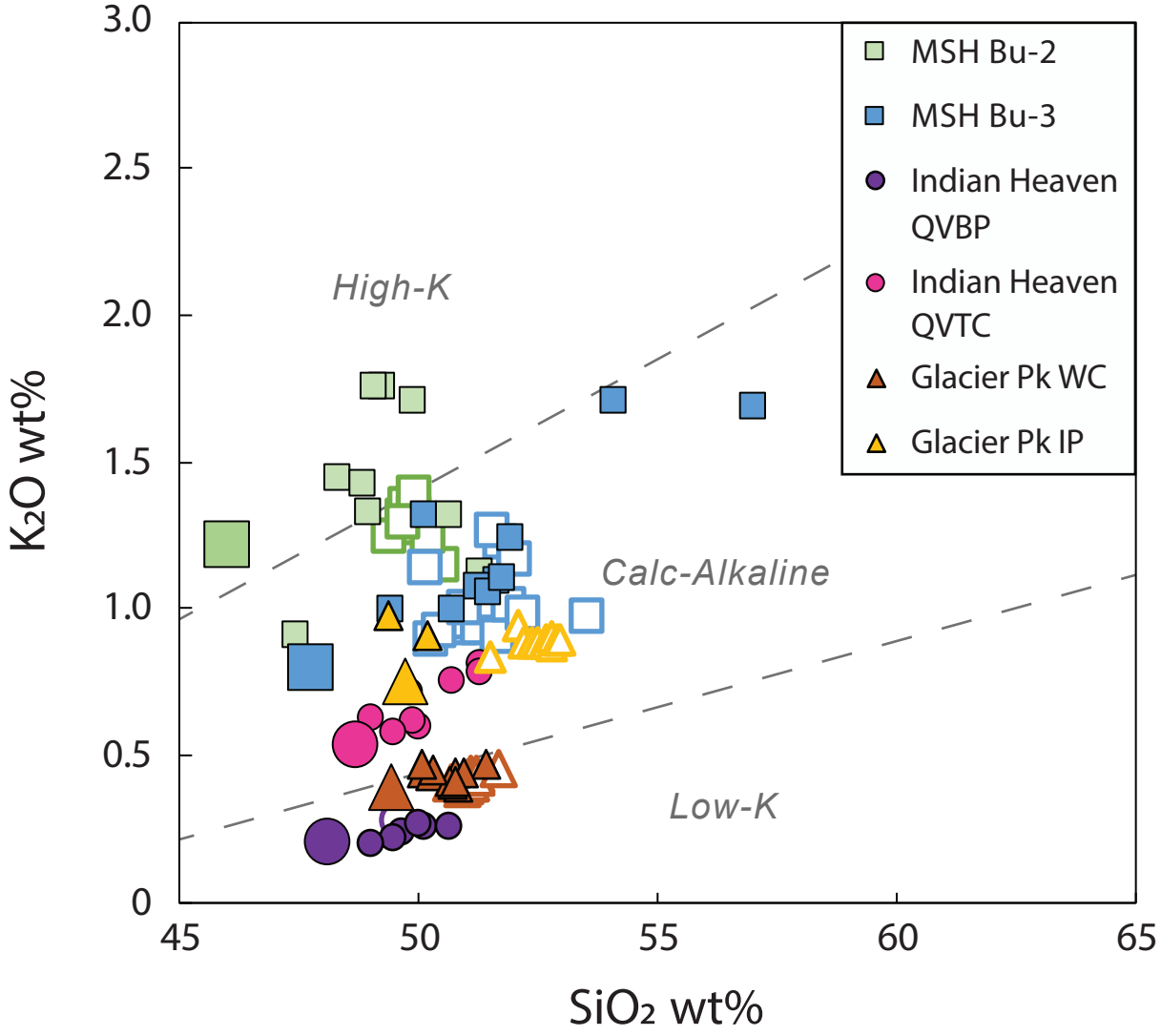
3.0
2.5
2.0
1.5
1.0
0.5
0
45
50
55
60
65
K2O wt%
SiO2 wt%
High-K
Calc-Alkaline
Low-K
MSH Bu-2
MSH Bu-3
Indian Heaven QVBP
Indian Heaven QVTC
Glacier Pk WC
Glacier Pk IP

Figure 3.

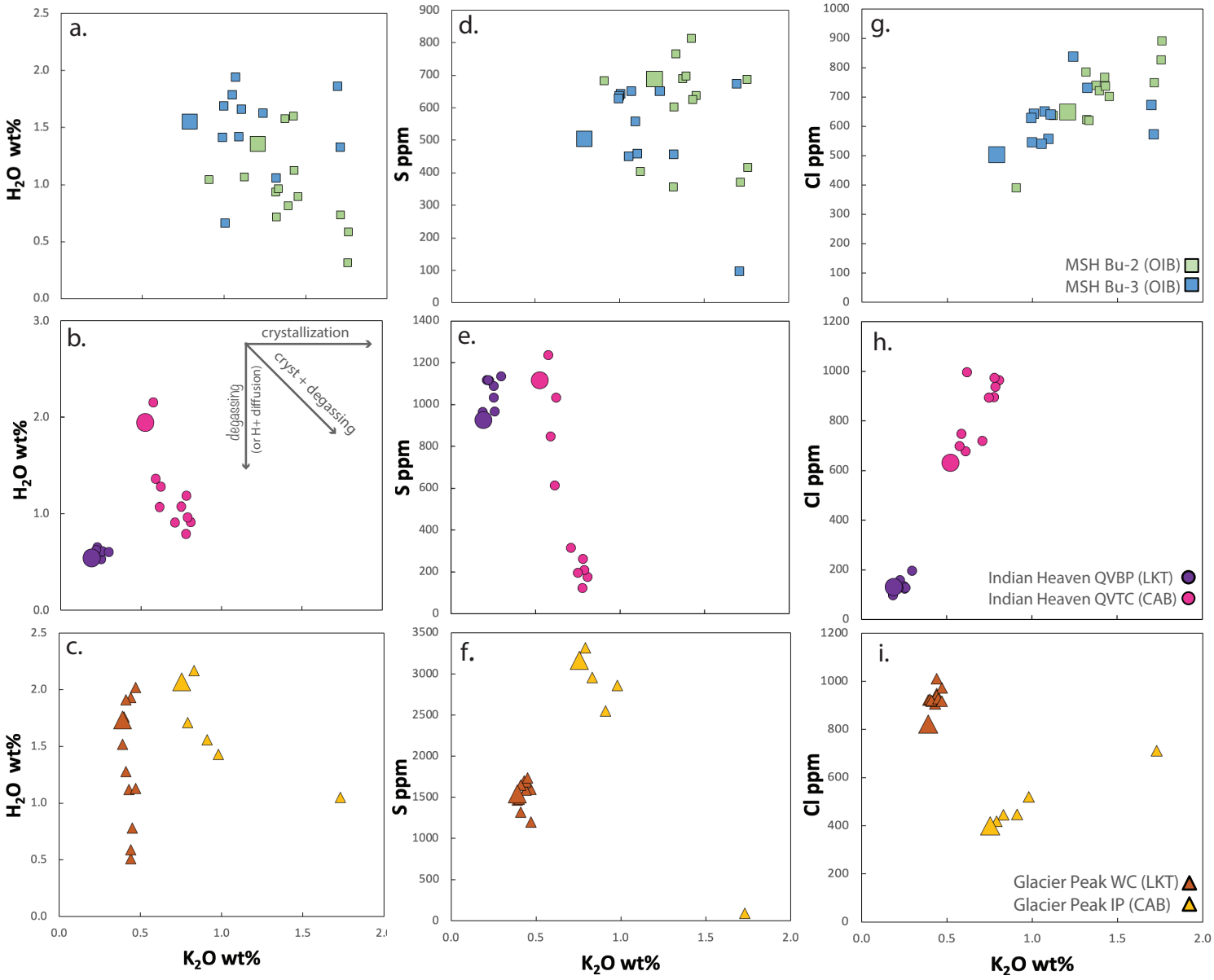
a.
b.
c.
d.
e.
f.
g.
h.
i.
H2O wt%
S ppm
Cl ppm
K2O wt%
crystallization
cryst + degassing
degassing
(or H+ diffusion)
MSH Bu-2 (OIB)
MSH Bu-3 (OIB)
Indian Heaven QVBP (LKT)
Indian Heaven QVTC (CAB)
Glacier Peak WC (LKT)
Glacier Peak IP (CAB)

Figure 4.

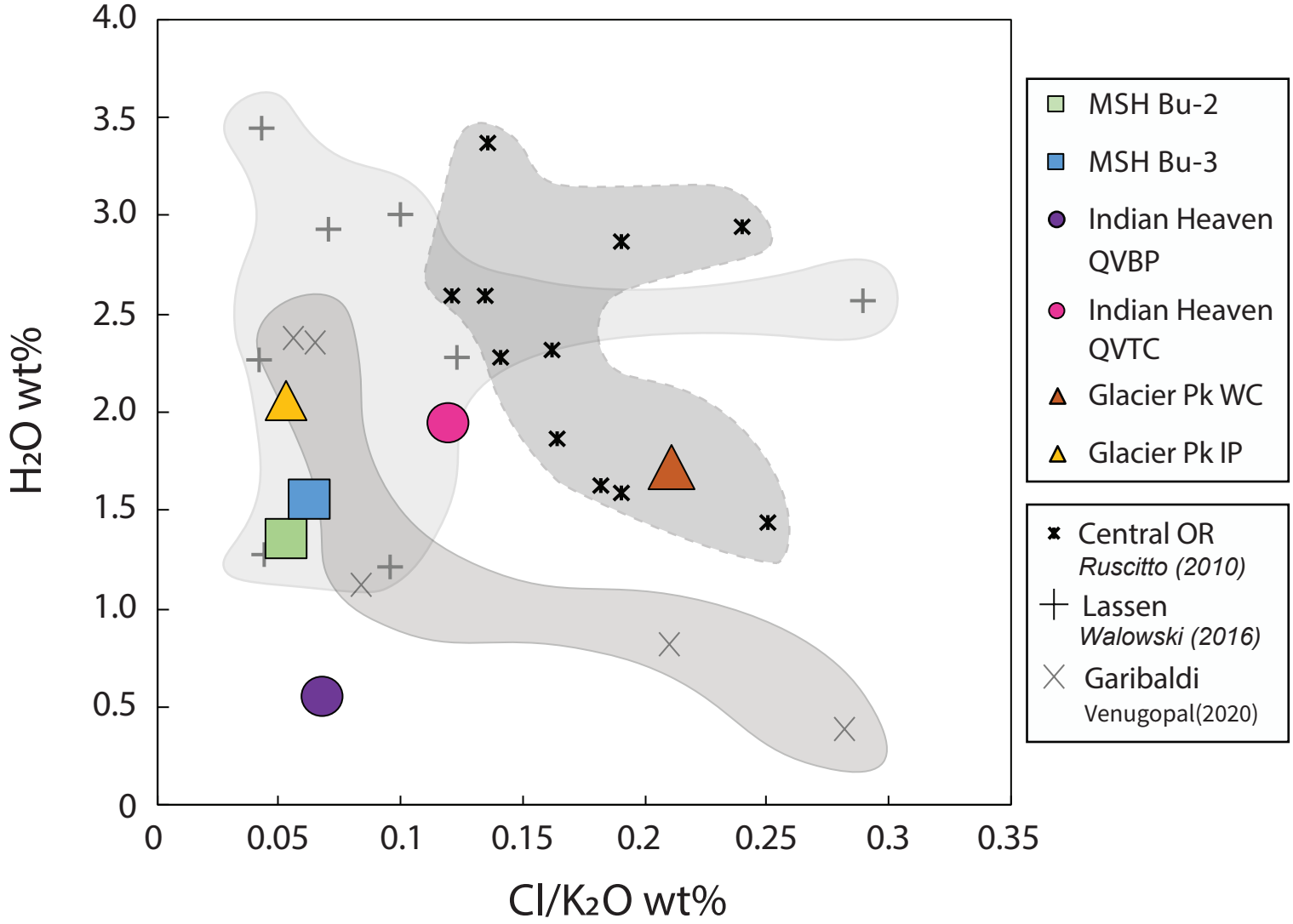
4.0
3.5
3.0
2.5
2.0
1.5
1.0
0.5
0
0
0.05
0.1
0.15
0.2
0.25
0.3
0.35
H2O wt%
Cl/K2O wt%
MSH Bu-2
MSH Bu-3
Indian Heaven QVBP
Indian Heaven QVTC
Glacier Pk WC
Glacier Pk IP
Central OR
Ruscitto (2010)
Lassen
Walowski (2016)
Garibaldi
Venugopal(2020)

Figure 5.

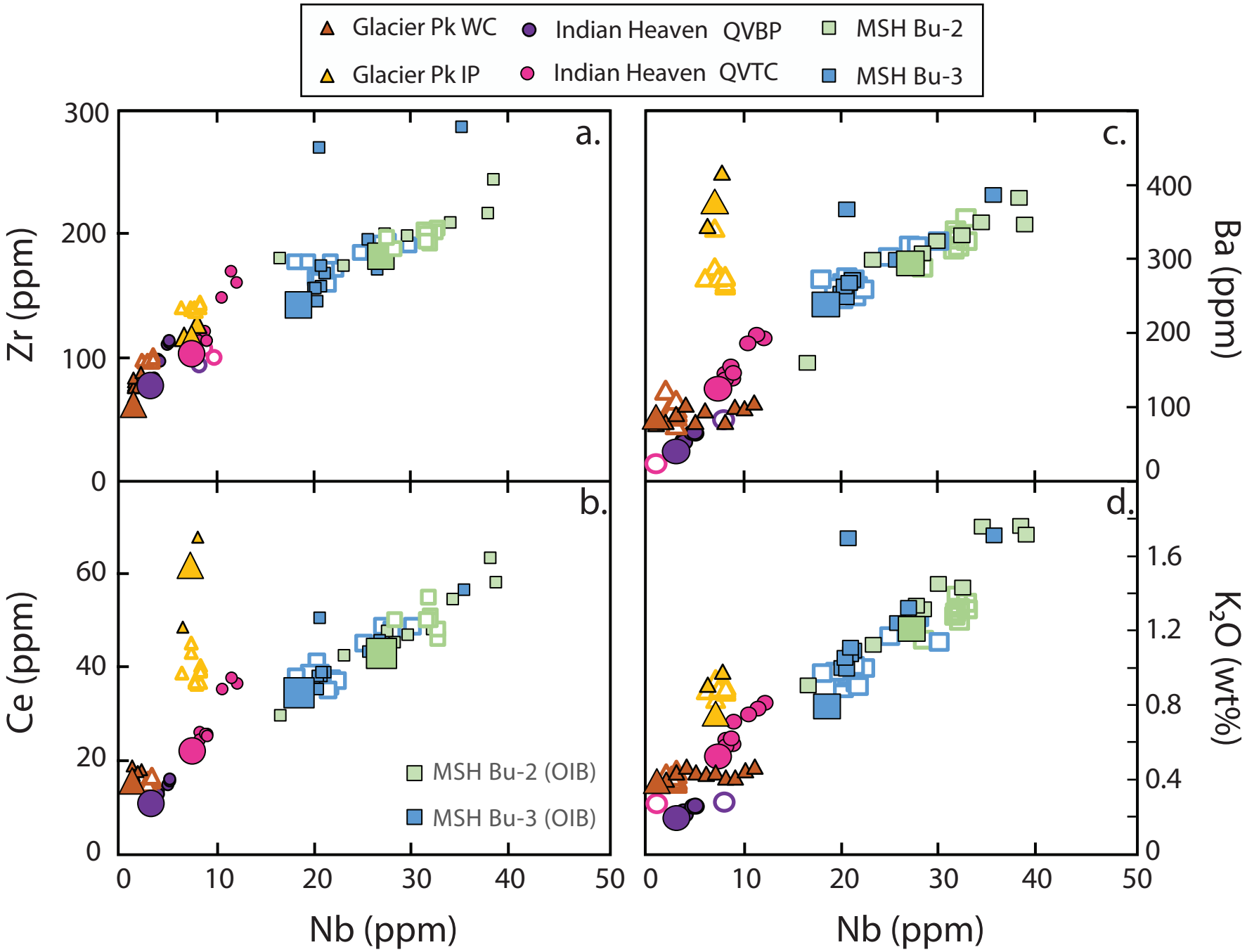
Glacier Pk WC
Glacier Pk IP
Indian Heaven QVBP
Indian Heaven QVTC
MSH Bu-2
MSH Bu-3
a.
b.
c.
d.
Zr (ppm)
Ce (ppm)
Ba (ppm)
K2O (wt%)
Nb (ppm)
Nb (ppm)
MSH Bu-2 (OIB)
MSH Bu-3 (OIB)
0
100
200
300
0
20
40
60
0
100
200
300
400
0
0.4
0.8
1.2
1.6
0
10
20
30
40
50

Figure 6.

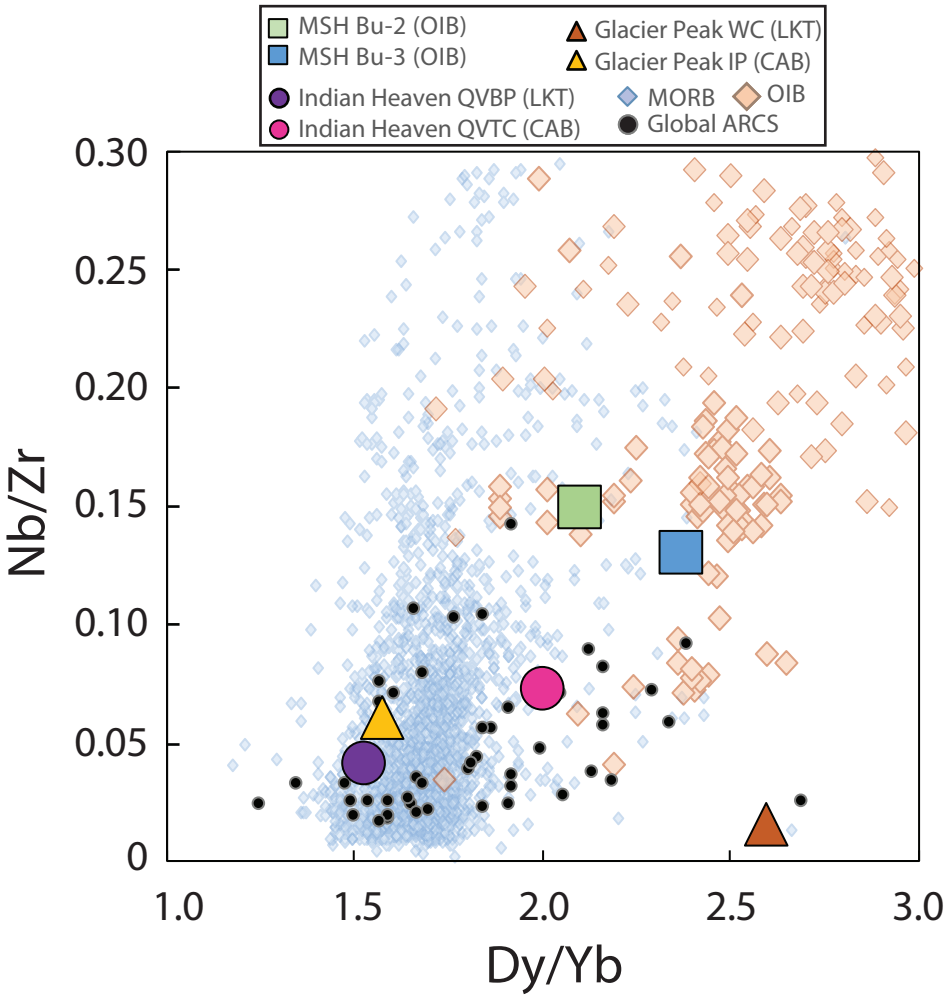
MSH Bu-2 (OIB)
MSH Bu-3 (OIB)
Indian Heaven QVBP (LKT)
Indian Heaven QVTC (CAB)
Glacier Peak WC (LKT)
Glacier Peak IP (CAB)
MORB
OIB
Global ARCS
0.30
0.25
0.20
0.15
0.10
0.05
0
Nb/Zr
1.0
1.5
2.0
2.5
3.0
Dy/Yb

Figure 7.

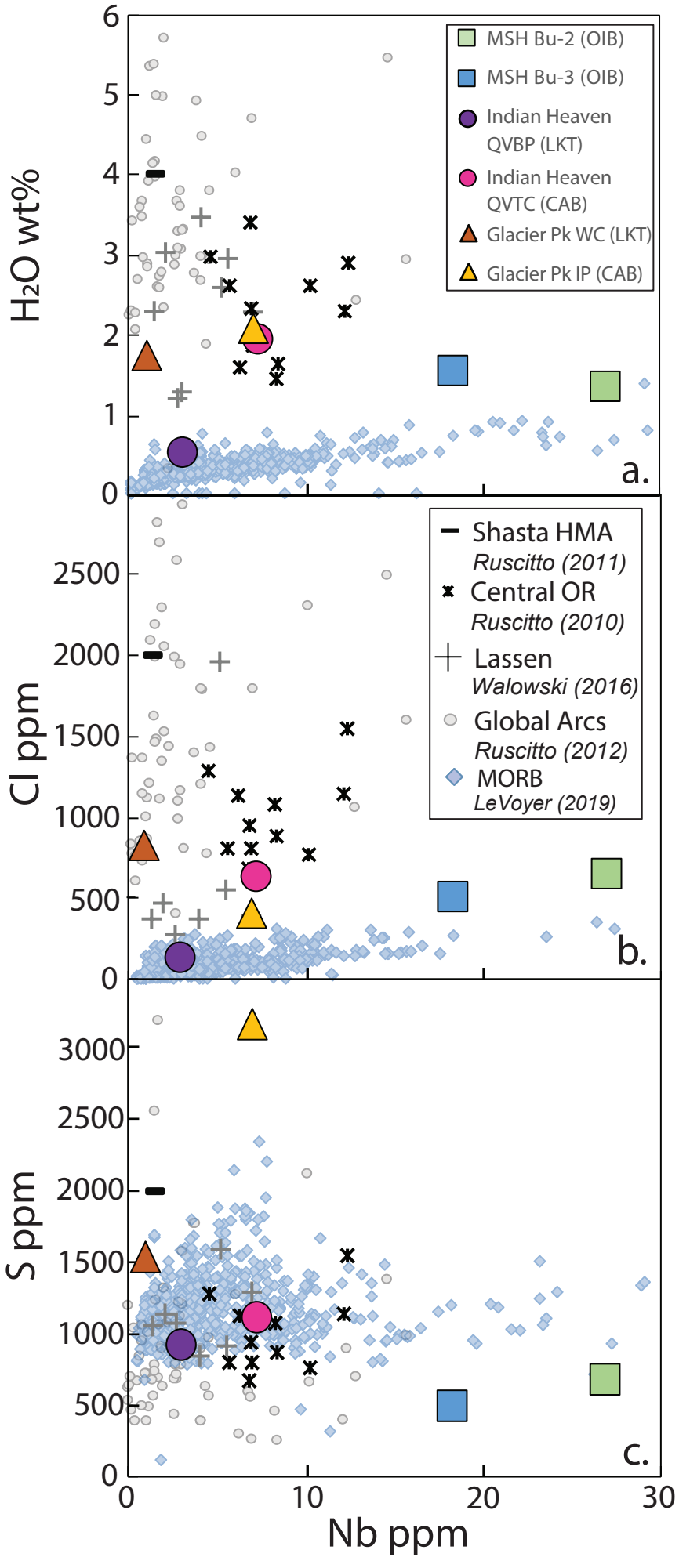
MSH Bu-2 (OIB)
MSH Bu-3 (OIB)
Indian Heaven QVBP (LKT)
Indian Heaven QVTC (CAB)
Glacier Pk WC (LKT)
Glacier Pk IP (CAB)
H2O wt%
a.
Shasta HMA
Ruscitto (2011)
Central OR
Ruscitto (2010)
Lassen
Walowski (2016)
Global Arcs
Ruscitto (2012)
MORB
LeVoyer (2019)
Cl ppm
b.
S ppm
c.
Nb ppm

Figure 8.

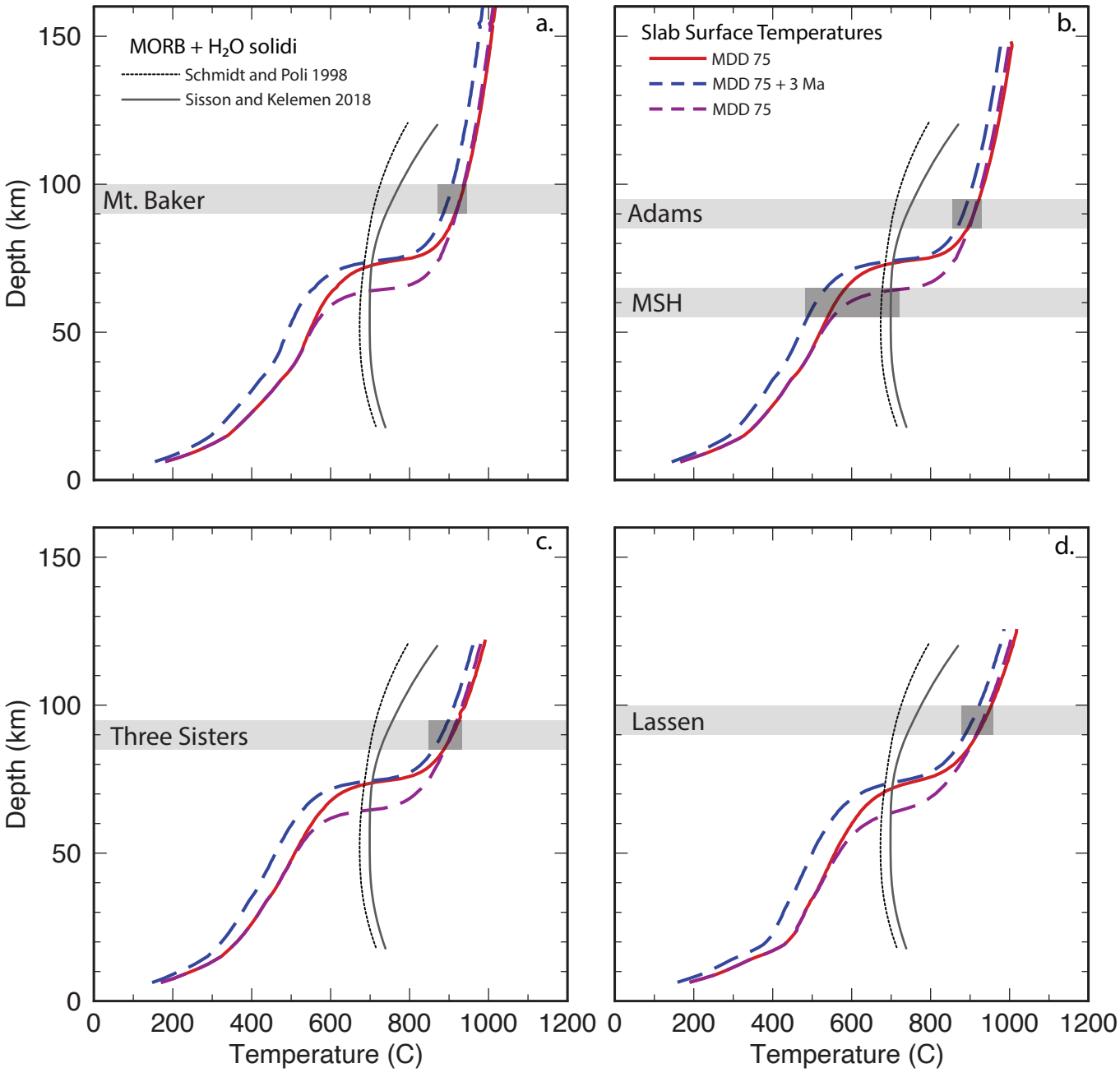
a.
MORB + H2O solidi
Schmidt and Poli 1998
Sisson and Kelemen 2018
Mt. Baker
b.
Slab Surface Temperatures
MDD 75
MDD 75 + 3 Ma
MDD 75
Adams
MSH
c.
Three Sisters
d.
Lassen
Depth (km)
Temperature (C)
0
50
100
150
200
400
600
800
1000
1200

Figure 9.

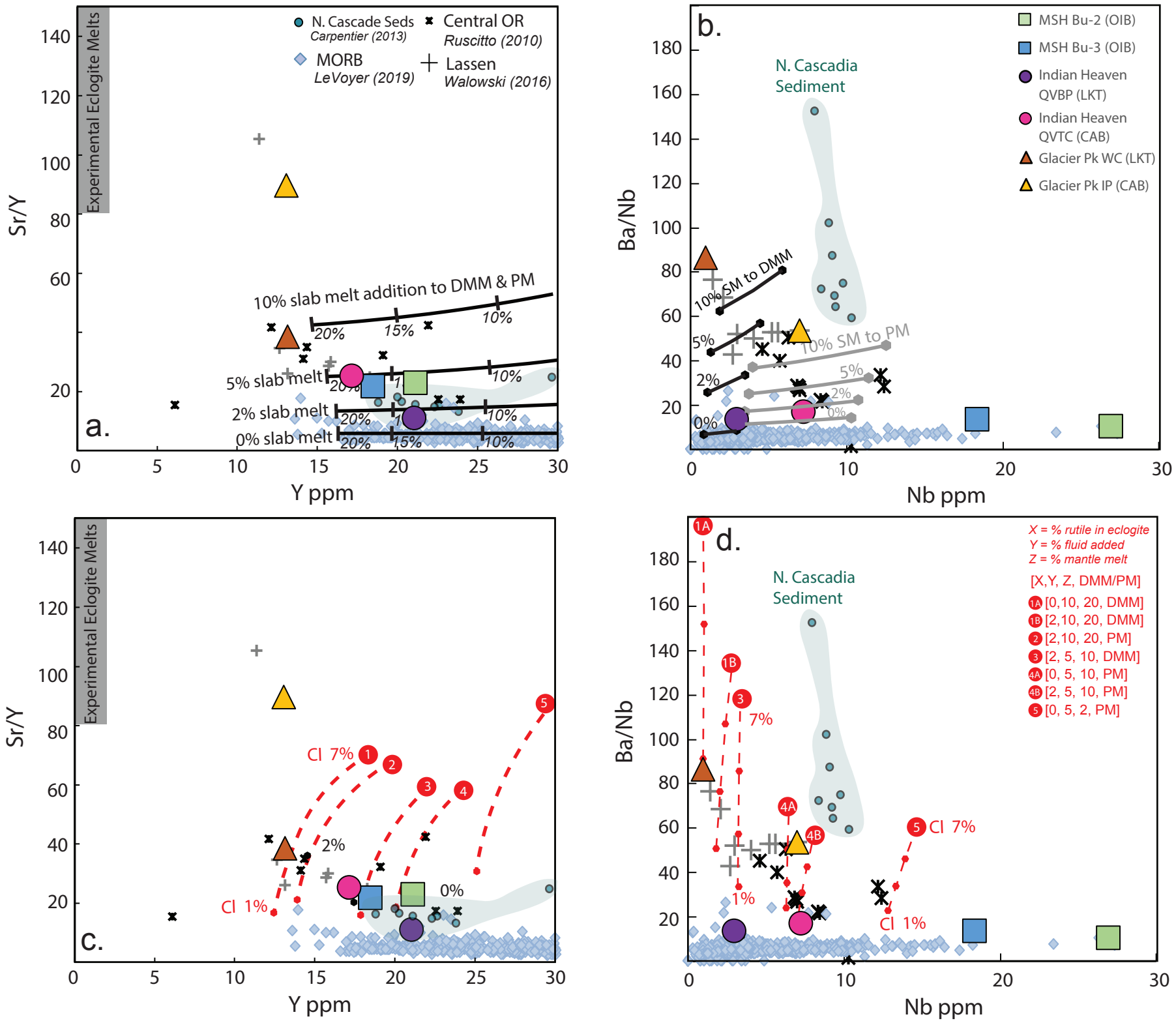
a.
Experimental Eclogite Melts
N. Cascade Seds
Carpentier (2013)
Central OR
Ruscitto (2010)
MORB
LeVoyer (2019)
Lassen
Walowski (2016)
10% slab melt addition to DMM & PM
5% slab melt
2% slab melt
0% slab melt
Sr/Y
Y ppm
b.
N. Cascadia Sediment
MSH Bu-2 (OIB)
MSH Bu-3 (OIB)
Indian Heaven QVBP (LKT)
Indian Heaven QVTC (CAB)
Glacier Pk WC (LKT)
Glacier Pk IP (CAB)
10% SM to DMM
10% SM to PM
Ba/Nb
Nb ppm
c.
Cl 7%
Cl 1%
2%
0%
d.
X = % rutile in eclogite
Y = % fluid added
Z = % mantle melt
[X,Y, Z, DMM/PM]
1A [0,10, 20, DMM]
1B [2,10, 20, DMM]
2 [2,10, 20, PM]
3 [2, 5, 10, DMM]
4A [0, 5, 10, PM]
4B [2, 5, 10, PM]
5 [0, 5, 2, PM]
7%
1%

Figure 10.

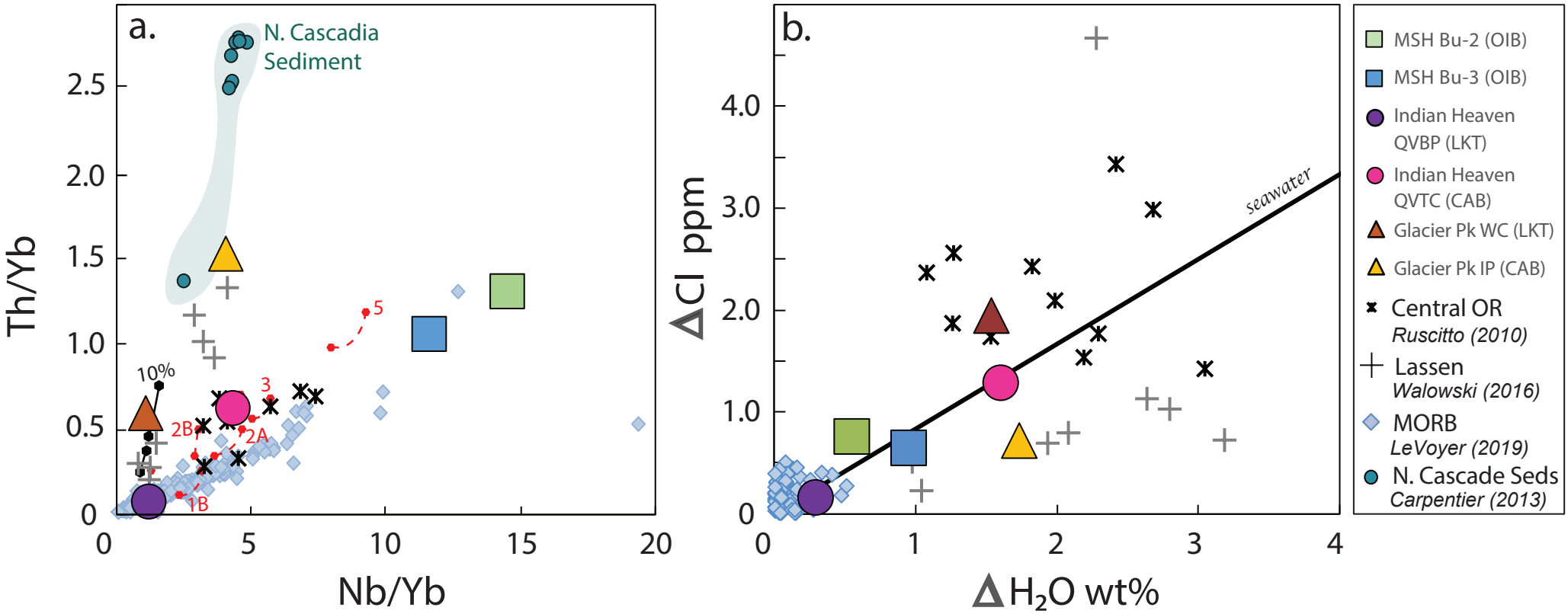
a.
N. Cascadia
Sediment
Th/Yb
Nb/Yb
0
0.5
1.0
1.5
2.0
2.5
0
5
10
15
20
10%
1B
2A
2B
3
5
b.
ΔCl ppm
ΔH2O wt%
seawater
0
1.0
2.0
3.0
4.0
0
1
2
3
4
MSH Bu-2 (OIB)
MSH Bu-3 (OIB)
Indian Heaven
QVBP (LKT)
Indian Heaven
QVTC (CAB)
Glacier Pk WC (LKT)
Glacier Pk IP (CAB)
Central OR
Ruscitto (2010)
Lassen
Walowski (2016)
MORB
LeVoyer (2019)
N. Cascade Seds
Carpentier (2013)